



Available online at www.sciencedirect.com

ScienceDirect

Geochimica et Cosmochimica Acta 281 (2020) 149–167

**Geochimica et
Cosmochimica
Acta**

www.elsevier.com/locate/gca

Ti-in-quartz: Evaluating the role of kinetics in high temperature crystal growth experiments

Marisa D. Acosta^{a,*}, James M. Watkins^a, Mark H. Reed^a, John J. Donovan^a
Donald J. DePaolo^b

^a University of Oregon, Department of Earth Sciences, 100 Cascade Hall, 1272 University of Oregon, Eugene, OR 97403-1272, USA

^b University of California, Berkeley, Department of Earth and Planetary Sciences, 307 McCone Hall, Berkeley, CA 97420-4767, USA

Received 2 February 2020; accepted in revised form 25 April 2020; Available online 8 May 2020

Abstract

We present results from 25 hydrothermal quartz growth experiments, all conducted at 800 °C and 1 kbar but with varying starting materials and run times, to address discrepancies between calibrations of the titanium-in-quartz (TitaniQ) thermobarometer. In our experiments, a gold capsule is loaded with silica glass, water, and either rutile or anatase as the TiO₂ source. In most experiments, there is also a large quartz seed crystal contained in an open inner capsule. The use of rutile versus anatase has a significant influence on the (re)crystallization pathways of the SiO₂ and TiO₂ components. When rutile is used, quartz overgrowths have abundant open cavities and complex zonations. The rutile does not completely dissolve because rutile is the stable TiO₂ polymorph, and yet, new rutile forms at the quartz seed-overgrowth interface and on the outer surface of quartz crystals. This suggests crystallization of quartz near $\Omega_{\text{rut}} \sim 1$, but wide-ranging Ti concentrations and zonations in quartz are indicative of kinetic effects. When powdered anatase is used, the quartz overgrowths look markedly different, lacking the open cavities and instead exhibiting step edges and terraces. The Ti concentrations in quartz from these experiments are also wide-ranging but reach larger values.

Our results span the range of previous calibrations and indicate that Ti concentrations in quartz are sensitive to the TiO₂/SiO₂ ratio of the fluid as opposed to the absolute concentration (or activity) of dissolved TiO₂. We present a kinetic model for quartz and rutile growth from a fluid where the input parameters are the initial degrees of supersaturation with respect to quartz and rutile, the total reactive surface area, and rate constants that link the degree of supersaturation to net precipitation rates. The model can explain many of the salient features of our experimental results, as well as those from previous studies, but requires that the rate constant multiplied by the reactive surface area for rutile is less than that of quartz, and that rutile solubility depends on the SiO₂ concentration of the fluid, as documented in the recent literature. Complete quartz-rutile equilibrium may not have been established in any of the experimental studies, but low-pressure experiments with slowly grown quartz seem to be more reliable than extrapolations from high-pressure experiments for thermobarometry of shallow natural systems.

© 2020 Elsevier Ltd. All rights reserved.

Keywords: TitaniQ; quartz; kinetic effects; Crystal growth; Hydrothermal

1. INTRODUCTION

The titanium-in-quartz geothermobarometer (TitaniQ) was developed by [Wark and Watson \(2006\)](#) and takes advantage of the broad occurrence of quartz in crustal rocks and its stability across a wide range of geological

* Corresponding author.

E-mail address: macosta@uoregon.edu (M.D. Acosta).

environments. Over the past decade, TitaniQ has been refined experimentally (Thomas et al., 2010; 2015) and applied by others to infer the conditions and rates of crystallization in volcanic and plutonic environments (Wark et al., 2007; Shane et al., 2008; Girard and Stix, 2012; Mercer and Reed, 2013; Ackerson et al., 2018; Chamberlain et al., 2014), metamorphic environments (Behr and Platt, 2011; Bergman and Piazolo, 2012; Ashley et al., 2013), and hydrothermal systems (Betsi and Lentz, 2010; Müller et al., 2010; Vasyukova et al., 2013; Tanner et al., 2013; Mercer and Reed, 2013).

A puzzling issue that has emerged from the widespread application of the Thomas et al. (2010) calibration of TitaniQ is that it yields temperature estimates that are systematically lower, by about 100–150 °C, than those given by other thermobarometers applied to the same rocks (Fig. 1a), especially in relatively low pressure environments (<3–4 kbar) where temperature can also be estimated by other methods. TitaniQ is based on principles of equilibrium partitioning, as applied to the experiments upon which TitaniQ is based, which were carried out at temperatures of 700 to 940 °C and pressures of 5 to 20 kbar. Thomas et al. (2010) were thorough in their analysis of run products and established multiple lines of evidence for having achieved quartz-rutile equilibrium in their experiments, including: (1) reproducible and systematic temperature- and pressure-dependences of Ti concentration in quartz, (2) homogeneous distributions of Ti in quartz, (3) inclusions of rutile in quartz, indicating co-precipitation, and (4) checking the results by doing thermal annealing experiments (Thomas et al., 2015). If the expressions of TitaniQ represent the equilibrium case, how do we interpret the systematic differences with other thermobarometers (Fig. 1a) and other insights derived from decades of study? Two issues emerge: one is whether equilibrium was established in the experiments or in nature, and the other concerns the extrapolation of higher pressure data to low pressures. A related point is that natural crystals typically grow at rates that are many orders of magnitude slower than those in laboratory experiments, and thus the role of kinetic effects in the experiments should be evaluated.

Other researchers have grown quartz in the laboratory at pressures ranging from 1 to 10 kbar and reported lower Ti concentrations, by a factor of 2–3, than predicted by TitaniQ (Huang and Audéat, 2012; Nachlas and Hirth, 2015). In none of these latter experiments has quartz-rutile equilibrium been convincingly established, and yet, when one applies to natural quartz the empirical expressions deduced from slow quartz growth experiments (Huang and Audéat, 2012), the temperature estimates agree with those from other thermobarometers, including those based on mineral and fluid inclusions in quartz (Fig. 1b).

Our goal in this study is to investigate the low-pressure region with experiments at 800 °C and 1 kbar using a range of different starting materials and experimental configurations. An important point is that different sources of SiO₂ and polymorphs of TiO₂ have been used as starting material in previous studies. Because anatase has a higher solubility than rutile, it yields a larger initial concentration of

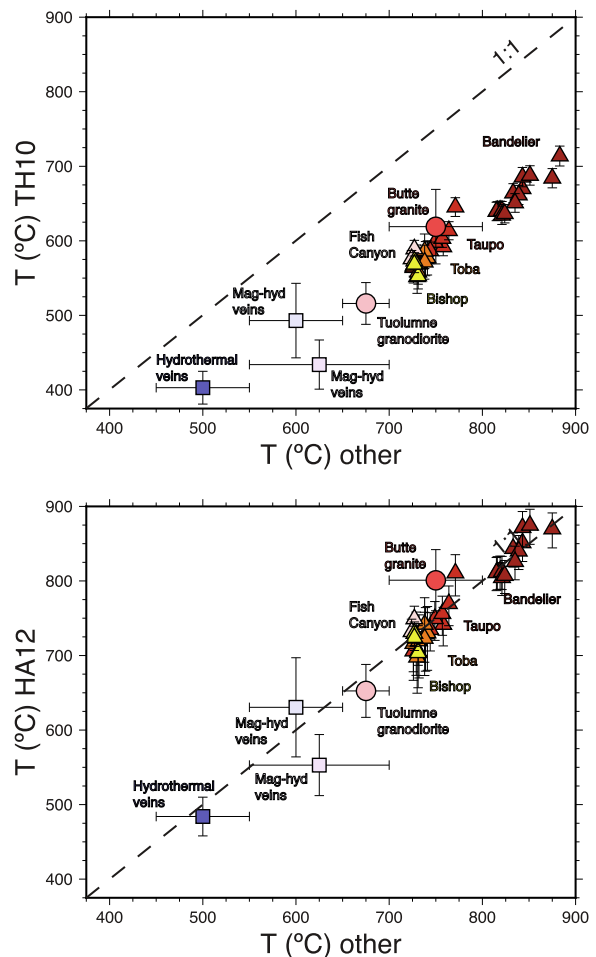


Fig. 1. TitaniQ applied to natural samples for which temperature has been estimated by other methods (Appendix A.1). Triangles are volcanic samples with zircon saturation temperatures based on quartz-hosted melt inclusion compositions along the same growth zones as entrapped zircons in the quartz crystals (Kularatne and Audéat, 2014). Circles are plutonic samples. Squares are hydrothermal quartz veins with rutile. For these latter samples, it is important to note that the Zr-in-rutile temperatures (Tomkins et al., 2007) from rutile within quartz veins are indistinguishable from the Zr-in-rutile temperatures from rutile in the alteration envelopes around quartz veins (Mercer and Reed, 2013). (A) The TH10 calibration yields temperatures that are systematically lower than those estimated using other geothermometers. (B) The HA12 calibration is in better agreement with the other geothermometers.

TiO₂ in the fluid phase than does rutile. As we show, anatase also has a surprisingly strong influence on the growth rate and morphology of the crystallizing SiO₂ component, suggesting a heretofore overlooked coupling between the SiO₂ and TiO₂ components. We use these new insights, combined with models of the evolution of the fluid phase composition during experiments, to evaluate the conflicting evidence from experiments and natural samples.

1.1. History of TitaniQ calibrations

Ostapenko et al. (1987, 2007) suggested that Ti in quartz could be used as a thermometer. Two decades later, the

TitaniQ geothermometer was calibrated experimentally by Wark and Watson (2006) using a piston cylinder apparatus at $P = 10$ kbar, temperatures ranging from 600 to 1000 °C, and durations of 3 to 17 days (66–406 h). At the time, Wark and Watson (2006) thought that the pressure dependency would be negligible but subsequent application of the 10 kbar calibration to natural samples yielded temperatures that were inconsistent with equilibrium mineral assemblages (e.g. Lowers, 2007; Ghiorso and Evans, 2008). Motivated by the possibility that such discrepancies could be due to a pressure-dependence, Thomas et al. (2010), hereafter referred to as ‘TH10’, ran similar experiments lasting 1–5 days at $P = 5$ –20 kbar and $T = 700$ –940 °C. Their results revealed that there is indeed a strong pressure dependence to TitaniQ (Fig. 2a).

To extend TitaniQ to lower pressures, Huang and Audéat (2012) ran quartz growth experiments lasting 3–10 days at $T = 600$ –850 °C and $P = 1$, 2, and 10 kbar. Their results are significantly different from those of the previous work (Fig. 2b). In the Huang and Audéat (2012) study, hereafter referred to as ‘HA12’, Ti concentrations are more variable, correlate positively with quartz growth rate, and are systematically lower than those of TH10. Because slower growth rates are generally indicative of a system closer to equilibrium, HA12 reasoned that the Ti concentrations from their slow-grown quartz crystals could be used as the basis of a new set of equilibrium calibration curves (Fig. 2b), which as shown in Fig. 1b, generally agree well where comparisons can be made with other temperature estimates. This implies that, the systematic nature of their results notwithstanding, the higher Ti-in-quartz from TH10 reflects far-from-equilibrium behavior.

The results of HA12 and interpretation therein led Thomas et al. (2015), hereafter referred to as ‘TH15’, to conduct thermal annealing experiments where they used quartz starting material with higher-than-equilibrium Ti contents. The overgrowths on their quartz seeds had lower Ti, by an amount that was consistent with their previous results at 20 kbar. This, along with the generally more sys-

tematic P and T dependence of their calibration, allowed them to make a case for why their experiments reached equilibrium whereas those of HA12 did not. They concluded that HA12’s low Ti concentrations were a consequence of large gradients in titania activity ($a_{\text{TiO}_2}^{\text{liq}}$) persisting throughout the runs.

1.2. Equilibrium partitioning relationships

TitaniQ is intended to apply to equilibrium between coexisting quartz, rutile, and a silicate or aqueous liquid. For slowly growing quartz crystals in natural rocks, an approximation to equilibrium may be attainable, but for rapidly grown crystals in laboratory experiments, it is not guaranteed.

The amount of TiO_2 incorporated into quartz crystals *at equilibrium* with a liquid at rutile saturation is described by the relationship:

$$\mu_{\text{TiO}_2}(\text{qtz}) = \mu_{\text{TiO}_2}(\text{liq}) = \mu_{\text{TiO}_2}(\text{rt}), \quad (1)$$

which states that the chemical potential of TiO_2 dissolved in quartz is equal to that of TiO_2 in rutile and the liquid. The quartz-rutile equality can be expanded to:

$$\begin{aligned} \mu_{\text{TiO}_2}^o(\text{qtz}) + RT \ln \gamma x_{\text{TiO}_2}(\text{qtz}) \\ = \mu_{\text{TiO}_2}^o(\text{rt}) + RT \ln a_{\text{TiO}_2}(\text{rt}), \end{aligned} \quad (2)$$

where μ is chemical potential, μ^o is chemical potential at a defined standard state, R is the gas constant (8.314 J mol⁻¹ K⁻¹), T is temperature in Kelvin, a is activity, x is mole fraction, and γ is the activity coefficient for TiO_2 dissolved in quartz as a solid solution constituent. This expression can be rearranged to the form:

$$\ln x_{\text{TiO}_2}(\text{qtz}) = \frac{\mu_{\text{TiO}_2}^o(\text{rt}) - \mu_{\text{TiO}_2}^o(\text{qtz})}{RT} + \ln a_{\text{TiO}_2}(\text{rt}) - \ln \gamma_{\text{TiO}_2}(\text{qtz}), \quad (3)$$

which is essentially identical to equation (4) of TH10, except that they used the notation “ k ” instead of “ γ ” for

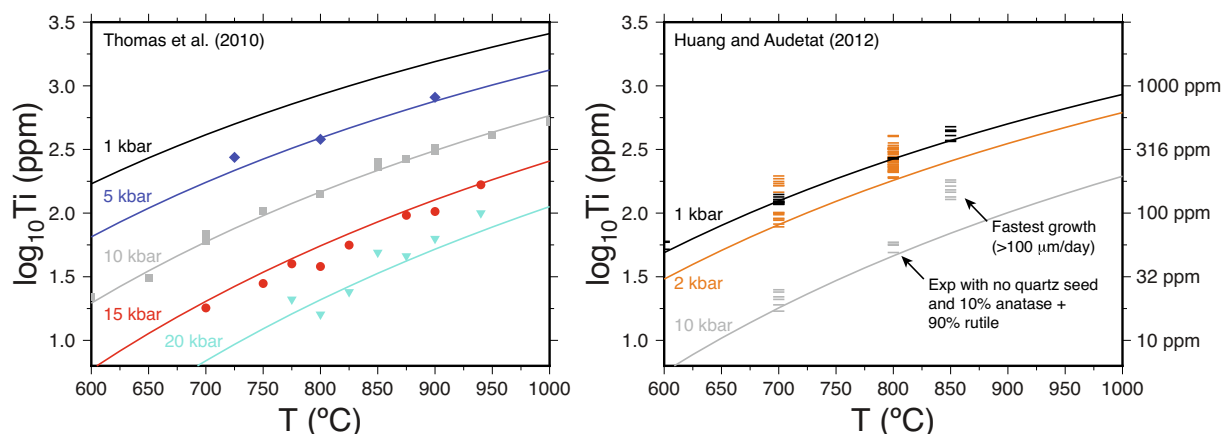


Fig. 2. Ti concentrations in quartz from Thomas et al. (2010) are higher and more systematic than those from Huang and Audéat (2012). The TH10 experiments were done with anatase as a source of titanium whereas the HA12 experiments used rutile with the exception of one experiment that used a mixture of rutile and anatase. The HA12 curves are based on their most slowly-grown quartz, which corresponds to the lowest Ti values.

the last term, where they referred to k as a Henry's Law constant. The first and last terms on the right-hand side of Eq. (3) have an unknown P - and T -dependence that can only be determined by experiment. Eq. (3) also states explicitly that if quartz and rutile coexist at equilibrium with a liquid, the mole fraction of TiO_2 in quartz is not dependent on the activity of TiO_2 in the liquid phase. When the system departs from equilibrium, Eq. (3) does not hold. For example, it is possible for quartz and rutile to grow simultaneously from a liquid phase where $\mu_{\text{TiO}_2}^{\text{liq}}$ is higher than the equilibrium value in both phases. And in general, if both quartz and rutile are growing at relatively high rates, both $\mu_{\text{TiO}_2}^{\text{liq}}$ and $\mu_{\text{SiO}_2}^{\text{liq}}$ are likely larger than the equilibrium solubility values. How much larger is the main question for interpreting the experimental results, since crystal growth, especially at laboratory experimental rates, is an inherently non-equilibrium process.

1.3. Requirements for maintaining equilibrium during quartz crystal growth

If quartz crystal growth in a laboratory experiment is not happening at near-equilibrium conditions, then the challenge is to estimate the SiO_2 and TiO_2 activities in the liquid phase during quartz and rutile growth. This is not necessarily an easy task, but a high degree of accuracy is not required. For example, the difference between the TH10 and HA12 TiO_2 concentrations in quartz at 10 kbar is about a factor of 3 (Fig. 2). If that difference results from a difference in $a_{\text{TiO}_2}^{\text{liq}}$, the liquid must be oversaturated with respect to rutile by a factor of three in TH10, undersaturated by a factor of three in HA12, or some other combination that leads to a factor of three difference between the two.

If the liquid is at rutile saturation, then $a_{\text{TiO}_2}^{\text{liq}} = K_{\text{sp,rut}}$ and the degree of supersaturation is given by $\Omega_{\text{rut}} = \frac{a_{\text{TiO}_2}^{\text{liq}}}{K_{\text{sp,rut}}}$, where $\Omega_{\text{rut}} > 1$ if the liquid is saturated in anatase, since anatase has a significantly higher solubility than rutile. Effective buffering of $a_{\text{TiO}_2}^{\text{liq}}$ at $K_{\text{sp,rut}}$ requires that rutile nucleation, growth, and dissolution are fast relative to quartz growth, despite being near rutile saturation, and that diffusion of TiO_2 in the liquid phase can efficiently erase any transient concentration gradients arising from the growth or dissolution of rutile and quartz. The complication in the quartz growth experiments of both TH10 and HA12 is that as quartz grew there likely was a continually changing $\text{TiO}_2/\text{SiO}_2$ ratio, and SiO_2 oversaturation in the liquid (without which the quartz would not grow). It is this issue we address below with models of what might be happening during the experiments.

2. METHODS

There are a number of challenges facing low pressure experiments that have been identified previously. TH10 attempted experiments at 1 kbar in cold-seal pressure vessels (CSPVs) but were unsuccessful in growing quartz large enough to analyse by electron probe microanalysis

(EPMA). When they used powdered quartz as starting material, the overgrowths were too small (<2 μm) for a microprobe, and when they used silica glass as starting material, it led to the formation of a mixture of polycrystalline cristobalite and tridymite. Another challenge is that EPMA measurements are susceptible to contamination by secondary fluorescence of Ti from rutile crystals, even if they are tens of microns away from the primary interaction volume (Wark and Watson, 2006; Borisova et al., 2018). These issues were circumvented by HA12 by using large quartz seed crystals that could be physically separated from the surrounding rutile. However, the HA12 experiments produced a wide range of Ti concentrations and Thomas et al. (2015) suggested that this aspect of the experimental design is fundamentally flawed and accounts for differences between the HA12 and TH10 calibrations.

2.1. Experimental capsules

Our experimental approach is a hybrid of those in TH10 and HA12. In most of our experiments, a 5 mm long Pt capsule (0.127 mm wall thickness) containing only a Ti-free quartz seed crystal is placed within a 15 mm long gold capsule (0.2 or 0.4 mm wall thickness) loaded with silica glass beads, 10 μL of de-ionized water and a TiO_2 phase (Fig. 3). The inner capsule mimics the conditions of the HA12 experiments, whereby a Ti-rich overgrowth forms on a large seed crystal. The outer capsule mimics the TH10 experiments, whereby quartz nucleates and grows in an environment where small TiO_2 particles are pervasive, which promotes buffering of $a_{\text{TiO}_2}^{\text{liq}}$. We also ran experiments without an inner capsule or quartz seed, but these produced mostly tridymite in runs lasting less than 10 days, confirming the behaviour documented by TH10 at low pressures. A select few of the newly formed quartz and tridymite crystals from double capsule and single capsule experiments were painstakingly separated from nearby TiO_2 and analysed using a novel combination of the plasma focused ion beam (PFIB) and EPMA (Appendix A.2 and A.3).

We initially planned to run experiments across a range of temperatures and pressures, but the variable results at 800 °C and 1 kbar warranted continued investigation under these conditions using different SiO_2 and TiO_2 starting materials (Table 1). In the end, the most important variables proved to be (a) whether quartz grew on a pre-existing seed or nucleated and grew through a series of metastable precursors and (b) whether the TiO_2 starting material was powdered rutile (99.9% purity; Alfa Aesar) or powdered anatase (99% purity; Sigma-Aldrich).

2.2. Experimental runs

Experiments were run in computer-controlled, rapid-quench cold-seal pressure vessels (CSPVs) at the University of Oregon. The capsules were placed in an Inconel rod, which was then inserted into a René 41 pressure vessel. The pressure vessel was connected to a stepper motor-controlled pressure line with H_2O as the pressure medium. Pressure was measured using a digital Omega pressure

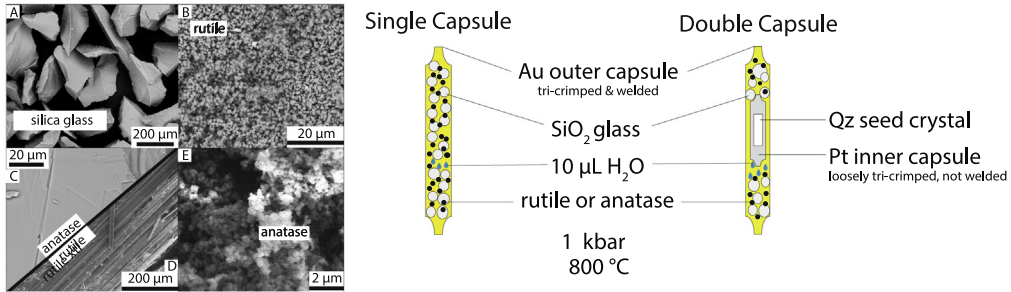


Fig. 3. Left: SEM images of starting materials: (A) sieved silica glass, (B) powdered rutile, (C) a single natural crystal of anatase showing a cleavage trace, (D) a single natural rutile crystal, and (E) powdered anatase. Note the particle size difference between the powdered rutile and powdered anatase. Right: Double-capsule and single-capsule designs used in this study.

transducer with a precision of ± 1 bar. Temperature was measured using a type K (chromel–alumel) thermocouple and was controlled to ± 2 °C.

To start a run, the pressure was brought up to 1 kbar and the pre-heated oven was lowered over the pressure vessel. The stepper motor controlled the pressure during heating. The desired temperature was reached after ~ 36 min. At this point we closed a valve to isolate the pressure vessel and turned off the stepper motor. This was done to mitigate pressure leaks along the pressure line but led to thermally induced pressure variations of about ± 10 bars throughout the run. To end the run, the sample was quenched slowly by raising the oven and allowing ambient air to cool the vessel. It took about 15 min for the pressure to drop to 1 bar and about 2 h for the sample to cool to 25 °C.

After an experiment, crystals were extracted from the capsules, imaged with a scanning electron microscope (SEM), mounted in epoxy, and polished to 0.25 microns using diamond grit. The polished surfaces were re-imaged prior to being analyzed on the microprobe.

2.3. SEM imaging

For most experiments, we collected SEM secondary electron (SE) and backscattered electron (BSE) images of quartz overgrowths from the inner capsule as well as the newly formed quartz crystals in the outer capsule. All crystals were imaged and analyzed at the Center for Advanced Materials Characterization in Oregon (CAMCOR) at the University of Oregon on an FEI Quanta 200 FEG Environmental SEM at 15 keV with a beam current of 400 nA.

The BSE and SE data were collected using the SEM in low-vacuum mode with variable water pressure (water pressure was increased if charging of the sample prevented adequate image collection). BSE imaging often produced a higher quality image than did SE, as it is less susceptible to charging. Once mounted and carbon-coated, SEM-cathodoluminescent (CL) images were collected under the same operating conditions but under high vacuum. Gain and offset vary from image-to-image and were optimized accordingly.

2.4. Raman spectroscopy

Phase identification was made with a Horiba Jobin-Yvon Labram 800 Raman spectrometer with a 5313-nm laser excitation and beam size of ~ 1 µm at Oregon State University. Spectra were analysed with the LapSpec 6.0 software suite. Each measurement was taken in the wavenumber range 50–850 cm⁻¹ using a 200 µm confocal hole diameter and 1200 lines-per-mm diffraction grating. After backgrounds were subtracted, peaks were fit with Gaussian functions identifying peak positions and attributes. The fitted spectra were compared to reference spectra from the RRUFF database.

2.5. PFIB sample prep of outer capsule materials

To escape the secondary fluorescence of proximal rutile in EPMA Ti analyses, quartz crystals were separated from rutile using a plasma focused ion beam (PFIB) at the University of Oregon (Appendix A.2). A Helios G4 PFIB UXe DualBeam SEM with a beam current of 0.5 µA was used to mill 70 µm deep moats around polished SiO₂ crystals. For some samples in which polishing would make it difficult to isolate crystals of certain morphology, the unmounted experimental run products were adhered to a carbon tab for PFIB extraction. After the crystal(s) of interest were identified, they were welded to the micromanipulator with C, removed from the sample, attached to a TEM holder and ion polished to a smooth, flat surface. We were then able to analyse these crystals by EPMA. Since this technique is time-consuming, only a few of the experimental run products were analysed in this manner.

2.6. Microprobe measurements

After SEM-BSE/SE/CL images were collected, Ti concentrations in quartz overgrowths were measured by electron probe microanalysis (EPMA) on a Cameca SX100 electron microprobe equipped with five tunable wavelength dispersive spectrometers. Operating conditions were 40 degrees takeoff angle, and a beam energy of 20 keV. The beam current was 100 nA and the beam diameter was 10

Table 1

Overview of experiments including capsule design and source materials used. Dashes and blank entries indicate no data. Images of quartz overgrowths are provided in [Appendix A.5](#).

Capsule Design	TiO ₂ source	Experiment	SiO ₂ sieve size (microns)	Duration (hours)	Min Ti (ppm)	Max Ti (ppm)	n	Outer Quartz Ti Range (ppm)
Double Capsule Experiments	Powdered rutile	2	>149	216	310	347	5	
	Powdered rutile	3	>149	214	288	315	5	
	Powdered rutile	4	>149	241	443	546	20	
	Powdered rutile	7B	175–104	189	288	513	17	
	Powdered rutile	8	249–175	260	357	482	11	
	Powdered rutile	9B	104–60	306	235	356	3	
	Powdered rutile	9C	104–60	247	216	570	17	458–562 (n = 3)
	Powdered rutile	15	175–104	314	275	443	19	629 (n = 1)
	Powdered rutile	18	175–104	288	272	454	10	
	Powdered anatase	19_ana	60–43	526	-	-	-	
	Powdered rutile	20	60–48	140	199	582	19	
	Powdered rutile	21	60–43	139	278	464	29	
	Single rutil xtl	24b	60–43	161	28	62	101	14–487 (n = 28)
	Single anatas xtl	27_ana	175–104	236	105	116	7	36–350 (n = 12)
	Powdered anatase	29_ana	175–104	169	126	248	23	177–890 (n = 18)
	Powdered anatase	31_ana	175–104	24	111	505	14	552–870 (n = 12)
	Powdered anatase	32_ana	175–104	6	275	419	8	
	Powdered rutile	33	175–104	24	211	215	2	
	Powdered rutile	34	175–104	6	416	673	9	
	Powdered anatase	Qzero_ana	175–104	-	-	-	-	
	Powdered rutile	Qzero	175–104	-	-	-	-	
Single Capsule Experiments	Powdered anatase	35_ana	175–104	400	608	952	9	
	Powdered rutile	36	175–104	170	437	582	2	
	Powdered anatase	37_ana	175–104	120	-	-	-	
	Powdered rutile	39	175–104	96	-	-	-	

or 5 microns. The data were reduced using ProbeForEPMA software.

The counting time was 425 seconds on-peak. Ti $\kappa\alpha$ was calibrated using a synthetic TiO_2 standard. When necessary, intensity data were corrected for Time Dependent Intensity (TDI) loss (or gain) using a self-calibrated correction for Ti $\kappa\alpha$. Ti $\kappa\alpha$ was measured on all five spectrometers and combined for quantitative analysis using the aggregate intensity method and correction for continuum artifacts using the quantitative blank correction (Donovan et al., 2011). The MAN background intensity data were measured on synthetic SiO_2 , MgO , NiO , and MnO standards and the Ti Ka background was corrected for continuum absorption (see Donovan et al., 2016). Unknown and standard intensities were corrected for dead time and standard intensities were corrected for beam and standard drift over time. The matrix correction method was the Armstrong-Brown $p(\phi z)$ method.

To avoid secondary fluorescence, areas selected for spot analysis were imaged with BSE when digitizing on the microprobe. A small number of spots ($n = 15$ out of 437) were identified as being contaminated by secondary fluorescence from a TiO_2 crystal beneath the surface and were therefore excluded from the final data set. The excluded data have Ti concentrations ranging from ~ 15000 to 35000 ppm. We also quantified the potential magnitude of secondary fluorescence contamination with Monte Carlo simulations of the geometries of our experimental run-products (Appendix A.3).

3. RESULTS

3.1. Titanium in quartz at 800 °C and 1 kbar

We observe variations in crystal form, TiO_2 abundance, and Ti zonation within quartz that depend on the type of TiO_2 source material and whether the quartz grows on the seed crystal (hereafter referred to as “inner quartz”) or nucleates and grows in the outer capsule (hereafter referred to as “outer quartz”). When powdered rutile is used, the inner quartz Ti varies from ~ 200 to 600 ppm, with many values clustering at or above the 267 ppm Ti calculated from HA12 (Fig. 4 – black symbols). When powdered anatase is used, the inner quartz has a similar range of ~ 150 –550 ppm Ti (Fig. 4 - blue symbols) whereas the outer quartz has higher and more variable Ti (~ 450 –850 ppm; Fig. 4 – open blue symbols). When a large single crystal of rutile or anatase is used, the inner quartz has low Ti (~ 50 –150 ppm) whereas the outer quartz has higher and more variable Ti (~ 50 to 500 ppm; Fig. 4 – orange and vermillion symbols). For single capsule experiments with no quartz seed crystal, the Ti concentrations in tridymite are higher in the anatase experiment than in the rutile experiment Electronic Annex.

3.2. Time series experiments (double capsule)

A series of short-duration experiments highlights the remarkably strong influence that powdered anatase versus powdered rutile has on the dissolution of SiO_2 glass as well as growth rates and shapes of SiO_2 polymorphs (Fig. 5). In the zero-time rutile experiment, the run products are indis-

tinguishable from the starting material. By contrast, the zero-time anatase experiment produced a mixture of cristobalite and source silica glass alongside anatase powder that has a larger grain size than the starting material. In both sets, outer silica appears to progress through the following Ostwald step rule sequence of metastable phases: glass-cristobalite-tridymite-quartz.

An important clue for interpreting the Ti results is that quartz and rutile crystallization in the outer capsule are considerably faster when anatase is used, suggesting high initial degrees of supersaturation in both components. A high initial degree of supersaturation with respect to rutile is supported by the direct precipitation and preservation of anatase in the 6-h experiment, as revealed by Raman spectroscopy (Appendix A.4). In the 24-h anatase experiment, the habits of outer quartz dipyramids are indistinguishable from those in the multi-day runs, suggesting that the reaction goes to near-completion sometime between 6 and 24 h. By contrast, the 24-h rutile experiment still contains incompletely dissolved silica glass and hexagonal platelets of tridymite in the outer capsule.

3.3. Multi-day powdered rutile experiments (double capsule)

Multi-day double capsule experiments using powdered rutile produced variable overgrowth thicknesses and Ti concentrations in quartz that overlap but extend the range produced in the HA12 experiments. Despite the variability, there are several generalizations that can be made. First, the inner quartz overgrowths always have abundant open cavities (incipient fluid inclusions) that run parallel to the c-axis of the overgrowth and are more filled-in near the intersections of crystal faces (Fig. 6a). Second, all the overgrowths are coated with small ($\sim 2 \mu\text{m}$) spherical to subrounded TiO_2 particles (Fig. 6a). When we observe TiO_2 encased within overgrowths after cutting and polishing, the TiO_2 is generally sparse, and occurs near the seed-overgrowth interface, akin to the experiments of HA12 (Fig. 6b). Third, nearly all the quartz overgrowths exhibit complex Ti zonations, as seen in SEM-CL images (e.g., Fig. 6c; Appendix A.5) and corroborated by EPMA analyses.

In the outer capsules, newly formed SiO_2 crystals are small (10–20 μm) and exhibit two morphologies: euhedral quartz dipyramids and subhedral hexagonal platelets identified by Raman spectroscopy as metastable tridymite (Fig. 6d). The relative abundance of the two polymorphs differs from experiment-to-experiment. In two of the experiments (9c and 15), the quartz dipyramids predominated, and a few of these crystals were extracted using the PFIB and then analysed by EPMA, yielding Ti-in-quartz values of ~ 450 –650 ppm (Fig. 4).

3.4. Multi-day powdered anatase experiments (double capsule)

The experiments using powdered anatase produced markedly different run products. The inner quartz lacks open cavities and instead exhibits step edges, terraces, and spiral growth features (Fig. 7a). In our first experiment using a 50:50 mixture of SiO_2 glass and anatase, the over-

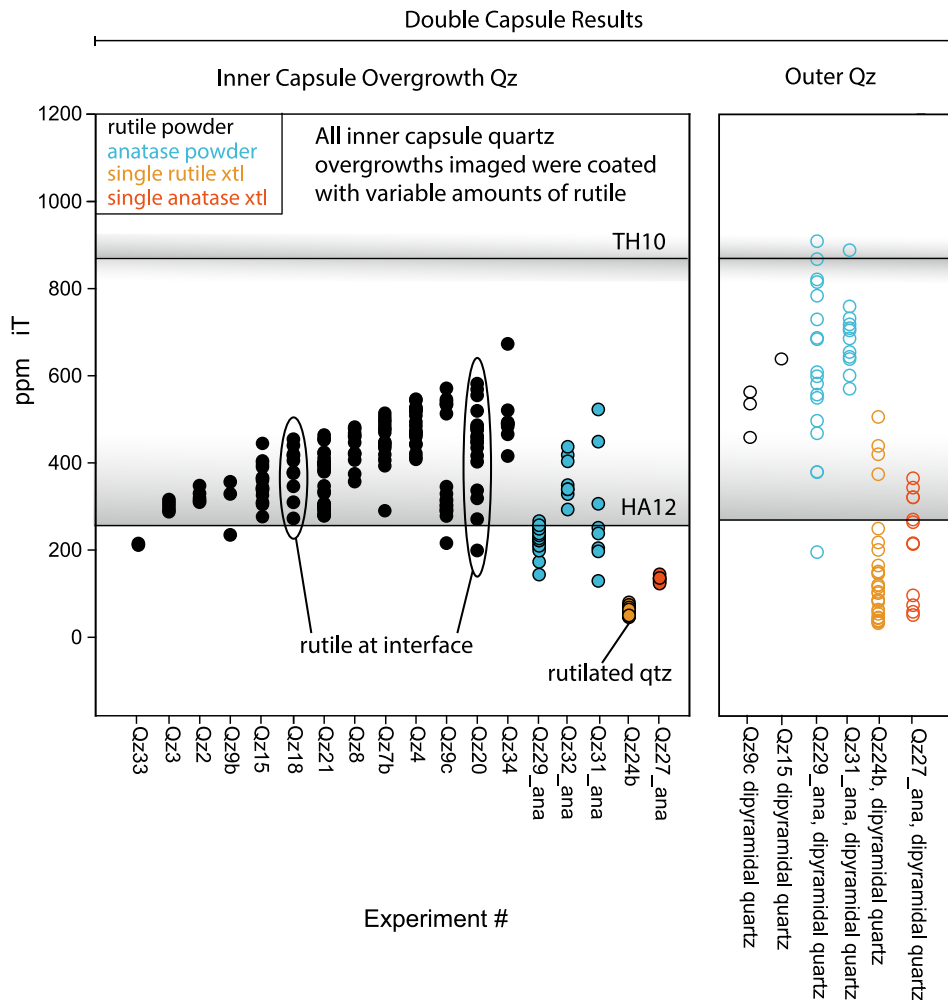


Fig. 4. Ti concentrations in quartz from each type of experiment (see legend), arranged in ascending order. Quartz overgrowths on the seed crystal are variable and below the values predicted by TH10. Dipyramidal quartz that nucleated and grew in the outer capsules also has variable but generally higher Ti values than inner capsule quartz. The single-capsule experiments (results not shown in the figure) produced mostly tridymite with sparse dipyramidal quartz, the latter of which are a target for future PFIB-EPMA analyses.

growth was so riddled with equant, relatively large (2–7 μm) TiO_2 crystals that we could not analyze it with EPMA. TEM-SAED analysis confirmed that the TiO_2 crystals were rutile but also revealed that the quartz lattice in the immediate vicinity of the TiO_2 inclusion was strained (Appendix A.4). Subsequent experiments were carried out using a 75:25 mixture of SiO_2 glass and anatase, which led to smooth overgrowths that lack TiO_2 inclusions and are relatively uniform in CL (Fig. 7b).

In the outer capsule, the newly precipitated quartz formed euhedral quartz dipyramids interspersed with euhedral TiO_2 crystals and some elongate rutile prisms (Fig. 7c). The outer quartz crystals show some variability in CL brightness (Fig. 7d) and have generally higher Ti concentration (~600–900 ppm) than the inner quartz from the same experiment (~150–500 ppm).

3.5. Large crystal experiments (double capsule)

The double capsule experiments in which we placed a single crystal of rutile or anatase in the outer capsule pro-

duce similar inner and outer quartz textures to those in the powdered rutile experiments, but a lower abundance of rutile precipitated during the run. Inner quartz exhibits open cavities (Fig. 8a) and zonations of Ti concentration (Fig. 8b). In the rutile crystal experiment, we found elongate TiO_2 micro-needles extending outward from the quartz overgrowth, forming a rutilated quartz overgrowth (Fig. 8c) with only 50 ppm Ti in a non-rutilated zone about 200 μm away.

The newly formed quartz in the outer capsule coated the large rutile or anatase crystal, the surface of which had barely dissolved during the run. In the anatase experiment, the surface of the crystal as viewed by SEM was highly altered from the initially flat anatase cleavage surfaces to a hummocky, irregular surface, a change presumably caused by the polymorphic transformation of anatase to rutile.

The lower abundance of rutile interspersed among the quartz crystals enabled us to measure Ti-in-quartz for both the inner and the outer crystals. In the outer capsule, the tridymite crystals are fairly homogeneous in CL and have Ti

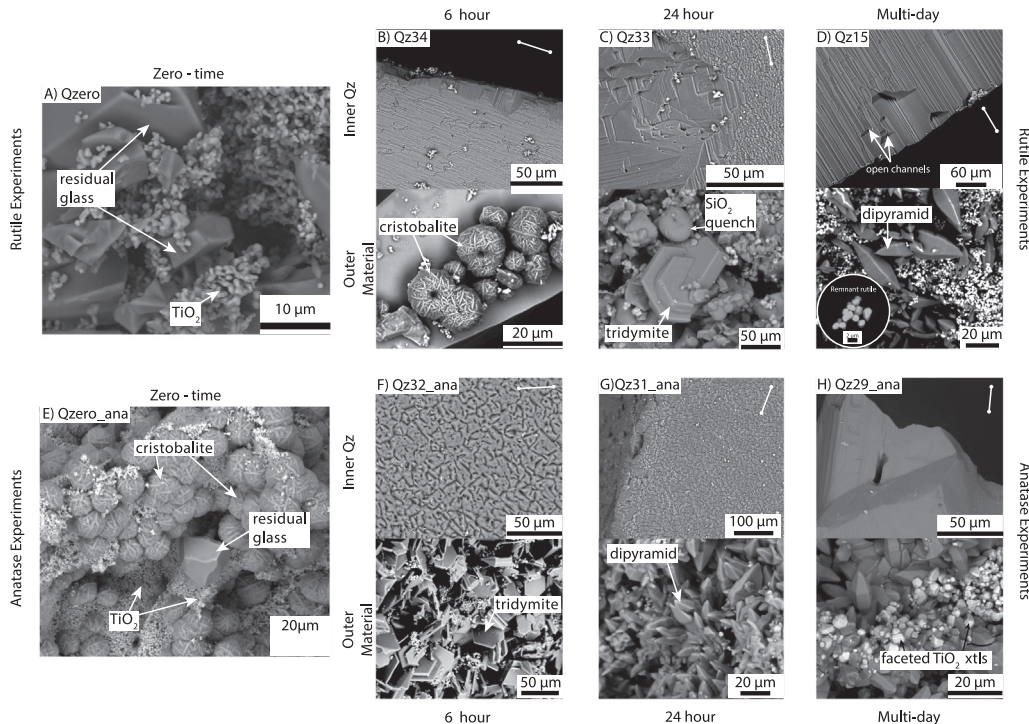


Fig. 5. Results from time series experiments performed with rutile powder (top) and anatase powder (bottom). Barbells in this and subsequent figures indicate the direction of the c-axis. (A) In a rutile experiment with no dwell, the end products are indistinguishable from the starting materials. (B-D) The inner quartz overgrowth has open channels parallel to the c-axis whereas the outer material crystallizes through the sequence cristobalite-tridymite-quartz. (E) In an anatase experiment with no dwell, cristobalite has already formed. (F-H) The inner quartz overgrowth has a rugose texture that evolves into a smooth surface lacking the c-axis channels. The outer SiO₂ material crystallizes through the sequence cristobalite-tridymite-quartz but does so more rapidly than in the rutile experiments. The outer TiO₂ material is a mixture of anatase and rutile in the 6-h run that evolves into relatively large euhedral rutile crystals in the multi-day runs.

between 237–430 ppm with an average of ~320 ppm Ti. The quartz dipyramids are more complex in CL (Fig. 8d), having a diffuse CL-bright core surrounded by a CL-dark mantle (~30–150 ppm Ti) that is truncated by a sharp, irregular boundary with a CL-bright rim (~410–430 ppm Ti).

3.6. Multi-day powdered rutile and powdered anatase experiments (single capsule)

Four experiments were carried out without an inner capsule or quartz seed crystal. The single capsule rutile experiments produced hexagonal platelets of tridymite with 437–582 ppm Ti ($n = 2$) (Fig. 9a and b). There were also sparse dipyramidal quartz crystals about 5–10 μm in diameter that we were unable to relocate for PFIB extraction. The newly precipitated TiO₂ particles are subhedral and exhibit a unimodal size distribution (Fig. 9b and 9c).

The single capsule anatase experiments produced tridymite as both hexagonal columns and 10–20 μm wedges (Fig. 9d and e). The Ti-in-tridymite values range from 608 to 952 ppm ($n = 9$). The newly precipitated TiO₂ particles exhibit a bimodal size distribution, with large, euhedral crystals (10–20 μm) alongside smaller (0.85–1.5 μm), anhedral to subrounded TiO₂ particles (Fig. 9f).

4. SIMPLIFIED KINETIC MODEL FOR THE TiO₂-SiO₂-H₂O SYSTEM

The wide range of textures, Ti concentrations, and CL zonations in quartz overgrowths produced in our single-capsule and double-capsule experiments is a clear manifestation of kinetic effects. Consequently, we need to evaluate the reaction kinetics of the TiO₂-SiO₂-H₂O system with consideration for how different starting materials could lead to different initial conditions and various Ti concentrations in quartz. In this section, we develop a kinetic model for a starting fluid that is quartz supersaturated and is under- or supersaturated with rutile, and that can evolve in composition during the experiment, to estimate whether these effects could account for the observations of our experiments, and what parameter values are implied. The model is an attempt to represent the dynamic nature of the experiments as opposed to assuming or asserting that equilibrium is attained in a subset of them. A key postulate is that the TiO₂/SiO₂ ratio of precipitated quartz depends on the TiO₂/SiO₂ ratio of the fluid, as opposed to simply the TiO₂ concentration (or $a_{\text{TiO}_2}^{\text{liq}}$). This is to be expected where a trace ion substitutes for a lattice ion (e.g., Mg/Ca or Sr/Ca in calcite; Tesoriero and Pankow, 1996; Gabitov and Watson, 2006; Nielsen et al., 2013), and there is strong

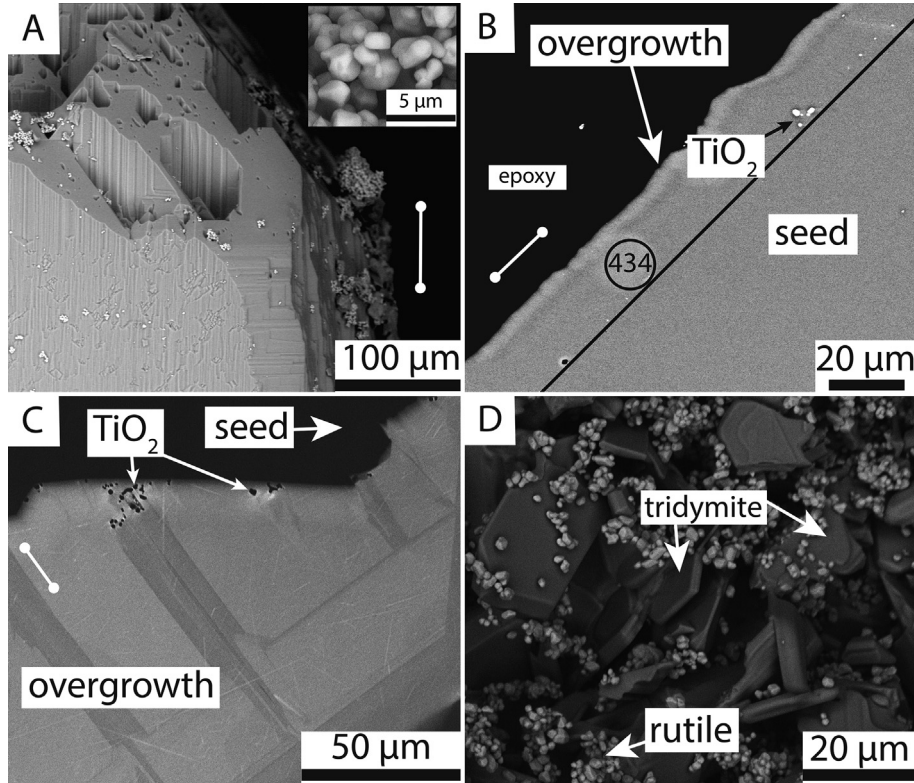


Fig. 6. Results from multi-day double-capsule runs using powdered rutile. (A) SE image of Qz21 showing the c-axis channels and rutile coating the outer surface of the overgrowth. (B) BSE image of Qz20 showing the polished overgrowth with rutile inclusions near the seed-overgrowth interface. The circle shows where a value of 434 ppm Ti was measured. (C) SEM-CL image of the polished Qz18 overgrowth showing rutile inclusions near the seed-overgrowth interface and complex zonation. (D) BSE image of Qz20, which is representative of outer capsule material in many of the multi-day runs. Exceptions are Qz15 and Qz9c, which yielded dipyratidal quartz as opposed to tridymite.

evidence that Ti⁴⁺ substitutes for Si⁴⁺ on the tetrahedral site in quartz (Thomas et al., 2010).

4.1. Governing equations

As quartz grows it excludes TiO₂ relative to SiO₂, so the TiO₂/SiO₂ ratio of the solution tends to increase even as quartz growth draws down the TiO₂ concentration. If quartz and rutile grow simultaneously, the fluid TiO₂/SiO₂ will differ from the value at quartz and rutile saturation, and the amount of the difference depends on the quartz and rutile precipitation rates. The faster quartz grows, and the slower rutile grows, the higher the TiO₂/SiO₂ ratio in the fluid becomes.

By taking the derivative of the fluid TiO₂/SiO₂ quotient, the rate of change of the fluid (TiO₂/SiO₂)_f (=r_f) is written as:

$$\frac{dr_f}{dt} = \frac{1}{[SiO_2]} \frac{d[TiO_2]}{dt} - r_f \frac{1}{[SiO_2]} \frac{d[SiO_2]}{dt}. \quad (4)$$

The rates of change of the individual concentrations are:

$$\frac{d[SiO_2]}{dt} = \frac{-R_{qtz}}{M_f} \quad (5)$$

and

$$\frac{d[TiO_2]}{dt} = \frac{-(R_{rutile} + r_f K_d R_{qtz})}{M_f}, \quad (6)$$

where R_i is precipitation rate in units of moles/s, M_f is the mass of the fluid in kg, [TiO₂] and [SiO₂] are concentrations in moles/kg. The partition coefficient, K_d = (Ti/Si)_{quartz}/(Ti/Si)_{fluid}, describes the TiO₂/SiO₂ partitioning between quartz and fluid (cf. McIntyre, 1963). Eq. (6) shows that both rutile and quartz growth act to lower [TiO₂].

Substituting (5) and (6) into (4) yields, after some rearrangements:

$$\begin{aligned} \frac{dr_f}{dt} &= \left(r_f - r_f K_d - \frac{R_{rutile}}{R_{qtz}} \right) \frac{R_{qtz}}{M_f [SiO_2]} \\ &\approx \left(r_f - \frac{R_{rutile}}{R_{qtz}} \right) \frac{R_{qtz}}{M_f [SiO_2]}. \end{aligned} \quad (7)$$

This equation shows that what happens to r_f during the experiment depends on where it starts and the relative rates of rutile and quartz precipitation during the run. Quartz should precipitate with r_{qtz} = K_d(TiO₂/SiO₂)_f; that is, in proportion to the fluid phase r_f whether K_d is an equilibrium or a kinetically controlled value. If r_f starts out close to the ratio of precipitation rates, then it should remain close to constant during a run. If r_f substantially exceeds that ratio, then it will increase monotonically at a rate that

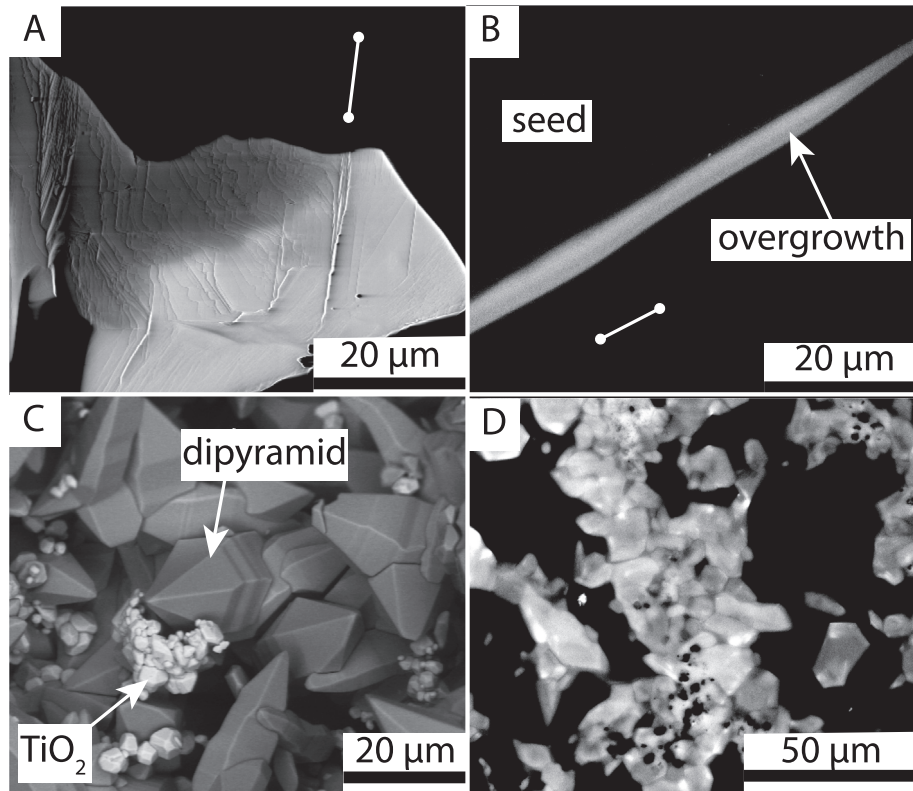


Fig. 7. Results from a multi-day double-capsule run using powdered anatase (Qz29_ana). (A) SEM image of the overgrowth showing growth terraces. The shadow is cast by a portion of the overgrowth not in the field of view (sample was tilted with respect to the electron beam). (B) SEM-CL image showing the smooth and continuous nature of the overgrowth in cross section. (C) BSE image showing outer quartz dipyramids co-existing with faceted TiO₂ crystals. (D) SEM-CL image of outer quartz. The boundaries of the crystals are “fuzzy” because of signal loss at the edges of the microcrystals. Dark equant spots scattered in the quartz cluster are TiO₂ crystals.

depends on the removal rate of SiO₂ from the fluid (the last term in Eq. (7) has units of s⁻¹ and is thus a timescale). However, if rutile is precipitating sufficiently fast, then r_f can decrease.

In the absence of diffusive transport limitations, the net precipitation rate of quartz and rutile can be written in the form (cf. DePaolo, 2011):

$$R_{\text{qtz}} = k_{f,\text{qtz}} A_{\text{qtz}} K_{\text{sp,qtz}}^* (\Omega_{\text{qtz}} - 1) = k'_{f,\text{qtz}} K_{\text{sp,qtz}}^* (\Omega_{\text{qtz}} - 1) \quad (8)$$

and

$$R_{\text{rutile}} = k_{f,\text{rut}} A_{\text{rut}} K_{\text{sp,rut}}^* (\Omega_{\text{rut}} - 1) = k'_{f,\text{rut}} K_{\text{sp,rut}}^* (\Omega_{\text{rut}} - 1) \quad (9)$$

where k_f is the forward rate constant for precipitation, A is the total mineral reactive surface area, K_{sp}^* is the stoichiometric solubility product (i.e., it is based on concentration and not activity), and Ω is the degree of supersaturation. It has been found experimentally that precipitation rates for other minerals such as calcite are not proportional to $(\Omega - 1)$, but rather, vary with this quantity raised to a power n . In the absence of experimental data for quartz, rutile, and anatase, we take the simplest approach and adopt Eqs. (8) and (9) for our calculations but note that other rate laws may prove more appropriate in the future. Additionally, we treat k'_f as constant with time even though the reac-

tive surface area is variable and k_f can also vary with Ω (e.g., De Yoreo et al., 2009).

The four input parameters required to calculate r_f as a function of time are $\Omega_{\text{qtz,initial}}$, $\Omega_{\text{rut,initial}}$, $k'_{f,\text{qtz}}$, $k'_{f,\text{rut}}$, and M_f . Since we don't know the absolute values of the rate constants, we fix $k'_{f,\text{qtz}} = 1.0$ and vary $k'_{f,\text{rut}}$ for the purpose of illustration. The value of M_f determines how long it takes for the system to relax back to equilibrium from the initially oversaturated state, but since we fix $k'_{f,\text{qtz}}$ at an arbitrary value of unity, it is sensible to remove M_f as a free parameter by normalizing the time by the total time. Finally, to convert r_f into a Ti in quartz value, it is necessary to specify a partition coefficient.

4.2. Estimating the partition coefficient

Previous studies on the solubility of Ti in quartz have not expressed the results in terms of partition coefficients, perhaps because it is difficult to estimate the amount of dissolved SiO₂ and TiO₂ in the liquid phase when the degree of supersaturation is unknown. A useful starting point is to estimate what the SiO₂ and TiO₂ concentrations would be if quartz and rutile were exactly at saturation and then speculate how much the TiO₂/SiO₂ ratio of the fluid might

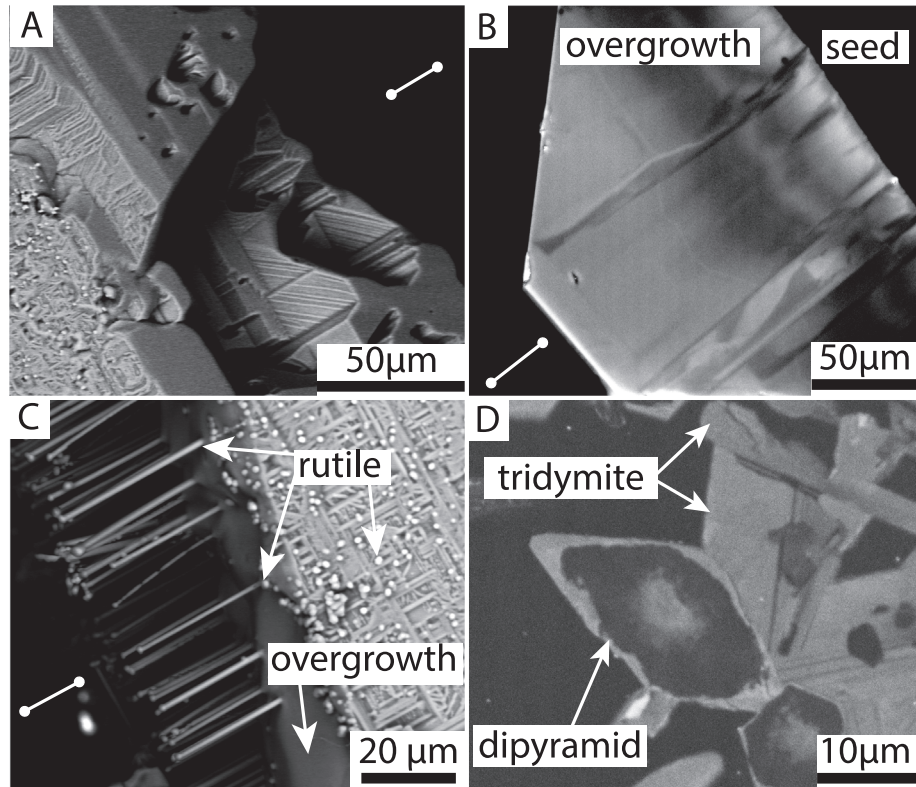


Fig. 8. A double-capsule multi-day experiment (Qz24b), where a large crystal of natural rutile was used as the source of TiO_2 yielded a rutilated overgrowth that had only 50 ppm Ti. (A) The quartz overgrowth exhibits striations and open cavities. (B) SEM-CL image showing wavy-oscillatory zonations on part of the overgrowth. (C) BSE image showing a portion of the overgrowth that was rutilated. (D) SEM-CL image showing zoned dipyramidal outer quartz coexisting with homogeneous hexagonal tridymite crystals.

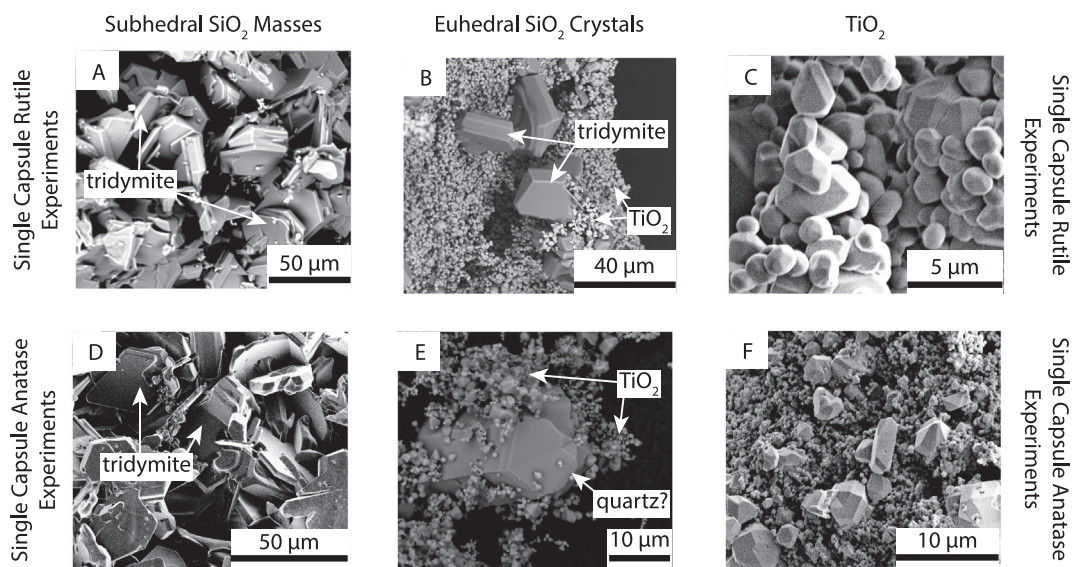


Fig. 9. SEM-BSE and SE images showing results from multi-day single-capsule experiments. Experiments done with rutile yielded both (A) polycrystalline, intergrown masses of euhedral-to-subhedral tridymite and (B) isolated, euhedral crystals tridymite in pockets of rutile. (C) Rutile from the single-capsule experiments developed facets with rounded edges. The single-capsule anatase experiments formed (D) polycrystalline masses of tridymite and (E) isolated euhedral crystals surrounded by TiO_2 . (F) In these experiments, was there a striking bimodal size distribution of TiO_2 .

change if the liquid were to have been highly supersaturated with respect to either or both of these phases.

The solubility of quartz in a hydrothermal solution at 800 °C and 1 kbar is $m_{\text{SiO}_2} = 0.048$ moles/kg-H₂O solvent as computed using SUPCRT92 (Johnson et al., 1992). This value is in good agreement with the value calculated using the expressions in Mysen (2019) for a TiO₂-SiO₂-H₂O fluid, which yields $m_{\text{SiO}_2} = 0.046$ moles/kg-soln.

The solubility of rutile is sensitive to fluid composition. While there is general agreement that rutile solubility increases with dissolved salt concentration, there is some disagreement concerning the effect of dissolved SiO₂. Antignano and Manning (2008) found no measurable increase or decrease on rutile solubility with increasing SiO₂ in two experiments at 800 °C and 10 kbar, whereas Mysen (2019) found a substantial (up to 3X) increase in rutile solubility in going from a TiO₂-H₂O fluid to a quartz-saturated TiO₂-SiO₂-H₂O fluid. At 800 °C and 1 kbar, the expressions of Mysen (2019) yield $m_{\text{TiO}_2} = 0.00113$ moles/kg-soln, or about 54 ppm Ti.

If quartz and rutile both precipitate exactly at saturation, the TiO₂/SiO₂ ratio of the fluid should be about 0.00113/0.048 = 0.024. For the solid TiO₂/SiO₂ ratio, a Ti in quartz of 850 ppm by mass (TH10) translates to molar TiO₂/SiO₂ = 0.00109, which is more than an order of magnitude lower than that in the liquid, meaning that quartz crystals are depleted in Ti with respect to the liquid ($K_d \sim 0.045$). A Ti concentration in quartz of 267 ppm (HA12) translates to an even lower $K_d \sim 0.014$. In what follows, we use $K_d = 0.014$ and assume K_d does not vary with the degree of supersaturation, i.e., there are no surface reaction-controlled kinetic effects (cf. Watson, 2004; DePaolo, 2011). Either or both assumptions may need to be relaxed in future iterations of the model.

4.3. Range of permissible supersaturation (Ω) values

The degree of supersaturation must be greater than unity to nucleate and grow a given phase. Upper bounds to the degree of supersaturation with respect to quartz and rutile can be estimated by considering the precursor phases and solubilities of the dissolving starting materials. Amorphous silica has a higher solubility than quartz by about a factor of 2, and the solubility of cristobalite is between that of quartz and amorphous silica (cf. Fig. 2 in Walther and Helgeson, 1977). The direct precipitation of cristobalite as a precursor to tridymite and quartz suggests an initial $\Omega_{\text{qtz}} > 1.5$ but we consider initial values of Ω_{qtz} from 1 to 2.

The solubility of anatase is not well known at temperatures above 325 °C, but it is certainly higher than that of rutile, possibly by a factor of three or greater based on extrapolation of lower temperature data (cf. Kalyani et al., 2015). We consider initial values of Ω_{rut} in the range of 0–4 depending on whether rutile or anatase is used as starting material. A value less than unity implies that rutile or anatase dissolution is slow and that the fluid reaches quartz saturation faster than it reaches rutile saturation.

4.4. Model behavior

Model outputs for different values of $k'_{\text{f,rut}}$ (relative to $k'_{\text{f,qtz}} = 1$) are shown in Fig. 10 to confirm the behavior of the model as described above. In all cases, the starting fluid is supersaturated in quartz. A lower initial Ω_{qtz} leads to a smaller range of Ti in quartz that is closer to the specified equilibrium value.

In Case 1–1, the fluid is initially undersaturated in rutile. According to Eqs. (5) and (6), [SiO₂] and [TiO₂] change at rates that depend on the respective k'_f values. The TiO₂/SiO₂ ratio of the fluid is initially low due to the high [SiO₂] and it increases monotonically because $r_f \gg R_{\text{rutile}}/R_{\text{qtz}}$ for all three values of $k'_{\text{f,rut}}$. In this version of the model, if the fluid starts below rutile saturation, it stays below rutile saturation because both rutile and quartz are sinks of TiO₂.

In Cases 1–2 and 1–3, the fluid is supersaturated with respect to rutile. When $k'_{\text{f,rut}} \ll k'_{\text{f,qtz}}$, the TiO₂/SiO₂ ratio increases during the period of quartz precipitation due to TiO₂ exclusion and then decreases as the effects of rutile precipitation take over. When $k'_{\text{f,rut}} = k'_{\text{f,qtz}}$, the TiO₂/SiO₂ evolves to the equilibrium value on the timescale of SiO₂ removal. When $k'_{\text{f,rut}} \gg k'_{\text{f,qtz}}$, the TiO₂/SiO₂ decreases on the short timescale of rutile precipitation and then increases back to the equilibrium value on the longer timescale of quartz precipitation. Importantly, if the fluid starts above rutile saturation, it stays above rutile saturation because the sink of TiO₂ to quartz is insufficient to drive the fluid to rutile undersaturation.

4.5. Modified kinetic model (Model 2)

The initial treatment using constant $k'_{\text{f,qtz}}$, $k'_{\text{f,rut}}$, $K^*_{\text{sp,rut}}$, and $K^*_{\text{sp,qtz}}$ implies that the TiO₂ and SiO₂ components operate nearly independently from each other. Such independence, however, is belied by the extent to which use of anatase instead of rutile as a starting material influences the initial dissolution and subsequent crystallization of the SiO₂ component. There is some guidance in the recent literature for how to incorporate TiO₂-SiO₂ coupling into the model parameters. Mysen (2019) showed that the solubility of rutile increases substantially as aqueous silica concentration increases from zero to quartz saturation, and it is plausible that rutile solubility may further increase as the fluid becomes increasingly supersaturated with respect to quartz; e.g.,

$$K^*_{\text{sp,rut}}(\text{moles kg-soln}^{-1}) = 0.00061 \cdot \Omega_{\text{qtz}} + 0.00052, \quad (10)$$

which describes a line going from rutile solubility in a TiO₂-H₂O fluid ($\Omega_{\text{qtz}} = 0$) through rutile solubility in a quartz-saturated a TiO₂-SiO₂-H₂O fluid ($\Omega_{\text{qtz}} = 1$) (Mysen, 2019).

Fig. 11 shows Model 2 outputs for the same three initial rutile saturation states shown in Fig. 10, given that $k'_{\text{f,rut}} \ll k'_{\text{f,qtz}}$. Case 2–1 shows that by incorporating the dependence of $K^*_{\text{sp,rut}}$ on Ω_{qtz} , an initial liquid that undersaturated in rutile can become supersaturated and new rutile

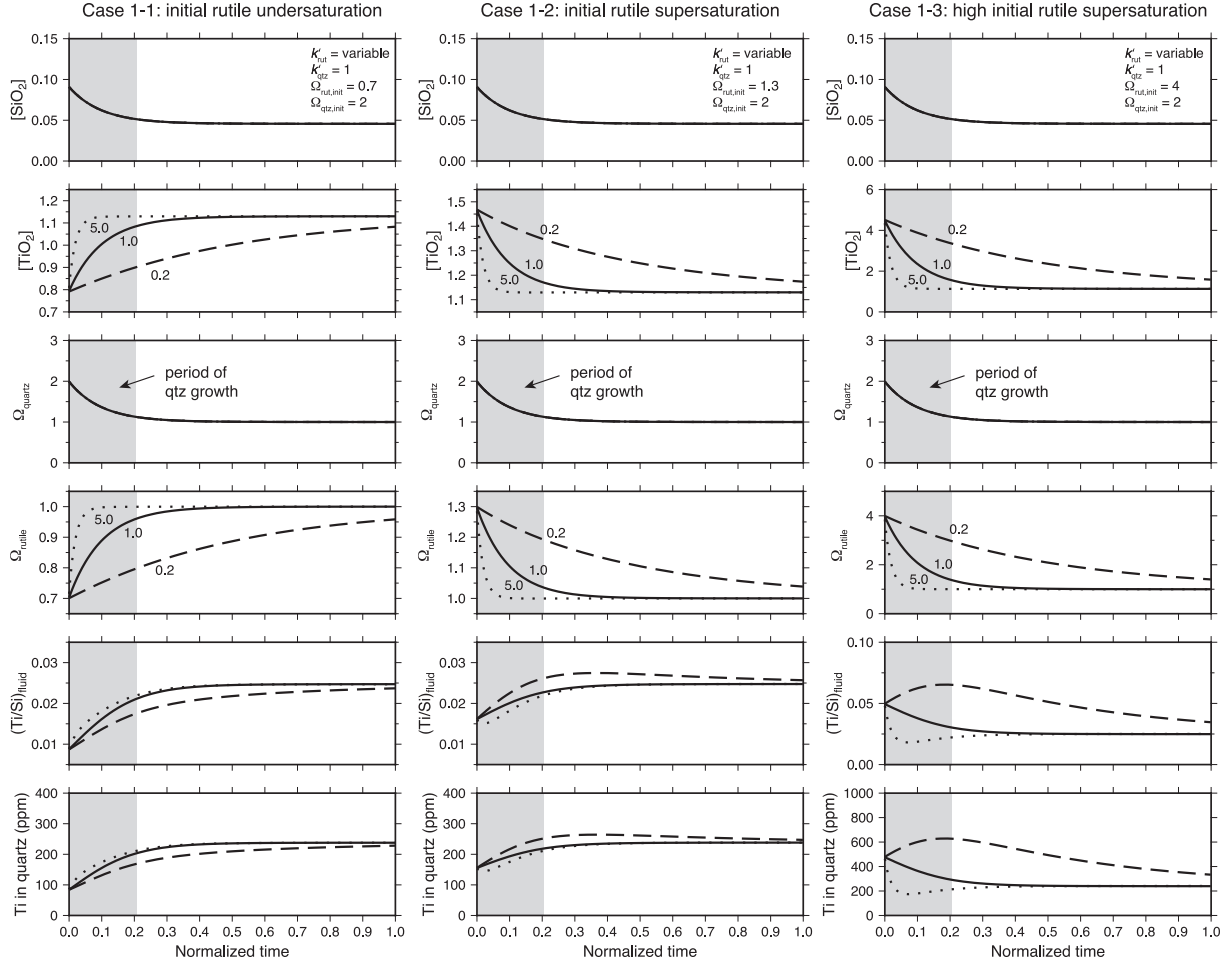


Fig. 10. Model results showing the evolution of SiO_2 and TiO_2 components for different $k'_{\text{f,rut}}/k'_{\text{f,qtz}}$ values. Because the absolute values of $k'_{\text{f,rut}}$ and $k'_{\text{f,qtz}}$ are not known, the simulated time is arbitrary and we therefore normalize the time by the time at the end of the run. In all cases, the fluid is supersaturated with respect to quartz. In Case 1-1, the fluid is initially rutile-undersaturated, the $\text{TiO}_2/\text{SiO}_2$ ratio of the fluid is low but increases monotonically as quartz precipitates and rutile dissolves. In Case 1-2, the fluid is less supersaturated in rutile than in quartz, and consequently, the initial $\text{TiO}_2/\text{SiO}_2$ is below the equilibrium value. When rutile precipitation kinetics are slow ($k'_{\text{f,rut}} = 0.2 k'_{\text{f,qtz}}$), the Ti in quartz slightly overshoots the equilibrium value before rutile precipitation brings it back down. In Case 1-3, the fluid is more supersaturated in rutile than in quartz, and consequently, the initial $\text{TiO}_2/\text{SiO}_2$ is above the equilibrium value. The $\text{TiO}_2/\text{SiO}_2$ either increases or decreases before adjusting to the equilibrium value depending on which phase is precipitating faster.

crystals can form. The outputs from Cases 2-2 and 2-3 show that the full range of Ti concentrations in quartz can be produced within the range of parameters we defined at the outset, provided that $k'_{\text{f,rut}} \ll k'_{\text{f,qtz}}$; i.e., that rutile is not serving as an effective buffer due to slow exchange with the fluid and/or low total reactive surface area.

5. DISCUSSION

Complete mineral-fluid or mineral-mineral equilibrium is difficult to establish in experiments where high supersaturations are necessary to grow crystals within hours to days, as is well known from lower temperature crystal growth experiments involving almost any mineral including quartz. In the following subsections, we discuss the ways that high temperature quartz growth experiments are affected by kinetics and ultimately conclude that,

whether rutile or anatase is used as starting material, experiments with slow quartz growth rates are needed to retrieve both the equilibrium values and the values exhibited by quartz grown at low degrees of supersaturation in nature.

5.1. Interpretation of our experimental results

Our experiments and modeling show that a wide range of Ti concentrations in quartz can be produced under isobaric and isothermal conditions. Although the model doesn't account for the complex dissolution and crystallization pathways we observe and for the non-constant total reactive surface areas (folded into the k'_f terms), it is useful for evaluating which experiments may have been closer to quartz-rutile equilibrium and interpreting the sign and magnitude of departures from equilibrium.

5.1.1. The low solubility of rutile is advantageous for bringing the liquid up to rutile saturation

The low solubility of rutile implies that only a small fraction of the starting material needs to dissolve to establish saturation initially or re-establish saturation after a perturbation. The post-run rounded TiO_2 particles in outer capsules are interpreted to be incompletely dissolved and partially recrystallized rutile powder because the particle size is smaller than or roughly equal to that of the starting material. In the outer capsules where rutile powder was well-mixed with SiO_2 , it is probable that quartz grew in an environment where $\Omega_{\text{rut}} \sim 1$ because the spacing between rutile particles is small and they are in close proximity to quartz.

5.1.2. Rutile is undersaturated in some parts of some of our experiments

The use of a single large crystal of rutile (Qz24b) or anatase (Qz27_ana) creates unfavorable conditions for a well-buffered liquid because the spacing between the large seed crystal and sparse, newly formed TiO_2 particles is high. Gradients in titania activity ranging from near zero to steep are likely responsible for producing Ti concentrations in outer capsule quartz that range from 14 ppm to 487 ppm. The exceedingly low Ti concentrations in the inner capsule (28 to 116 ppm), which overlap the low values of outer quartz from the same experiments, suggest quartz growth from a rutile-undersaturated inner capsule fluid. Rutile needles protruding from the Qz24b overgrowth (Fig. 8c) may have nucleated and grown towards the end of the period of quartz supersaturation and growth (Case 2-1 in Fig. 11).

5.1.3. Once the fluid is rutile-saturated, it stays rutile saturated

The lack of rutile in quartz overgrowths does not necessarily imply quartz growth from a rutile undersaturated liquid; it only implies that the liquid was below the critical supersaturation required to nucleate rutile. In two of the experiments (Qz18 and Qz20), which agree with the results of HA12, we found newly formed rutile as inclusions near the seed-overgrowth interface. This suggests that a critical degree of rutile supersaturation was reached early in those experiments, and the next immediate question is whether the lack of rutile in later-formed overgrowth implies that the fluid became undersaturated in rutile, as suggested by TH15.

To determine whether a rutile-saturated fluid can become undersaturated, we ran the model with a low $\Omega_{\text{rut}} = 1.1$ and low $k'_{\text{f,rut}}$ to isolate the effects of quartz growth on TiO_2 component. We find that quartz-driven rutile undersaturation requires an extremely high $\Omega_{\text{qtz}} \sim 5$ and a K_d that is an order of magnitude greater than we estimate (Fig. 12). Even with these parameters, the degree of undersaturation is minor (0.95) while the $\text{TiO}_2/\text{SiO}_2$ ratio is so high that it predicts Ti in quartz ~ 2200 ppm. The conclusion we draw is that once the fluid is saturated with respect to rutile, it should remain at or above saturation because neither quartz nor rutile growth is sufficient to drive the liquid to rutile undersaturation. We thus inter-

pret the lack of rutile in most of the overgrowths as reflecting a liquid that is near saturation but below the critical supersaturation required to nucleate new rutile crystals.

5.1.4. Anatase promotes higher initial Ω_{rut}

When anatase is used as starting material, it should either dissolve and reprecipitate as rutile or convert directly to rutile via a solid–solid recrystallization pathway on a timescale of tens of minutes to tens of hours, depending on factors such as temperature, pressure, adsorbed impurities, particle size, the abundance of TiO_2 particles, and the amount of dissolved silica (Shannon and Pask, 1965; Zhang and Banfield, 1999; Okada et al., 2001; Gouma and Mills, 2001; Hanaor and Sorrell, 2011; Sabyrov et al., 2013). Anatase, a more soluble polymorph than rutile, dissolves quickly and is capable of establishing an initially very high Ω_{rut} , as evidenced by our 6-h run where anatase precipitated directly from the liquid. A high initial aqueous TiO_2 concentration is consistent with higher Ti in outer-capsule quartz, reaching values > 850 ppm, than in experiments using rutile as starting material (450–650 ppm; $n = 4$).

5.2. Kinetic effects in HA12 and TH10

The kinetic models show that there are many conditions that could promote Ti heterogeneity in the quartz crystals, but also conditions where relatively homogenous crystals can be grown far from equilibrium. The Ti in quartz variations among our run products span a broader range than those of HA12, and while our minimum Ti values in rutile-bearing overgrowths (Qz18 and Qz20) are comparable to their minimum Ti values (~ 267 ppm at 800°C and 1 kbar), our results extend the high end of the range. HA12 used a single quartz crystal that dissolved at one end and precipitated at the other, thereby ensuring that quartz grows at relatively low degrees of supersaturation from a fluid that is near rutile saturation (Cases 2-1 and 2-2). Our higher values can be attributed to our use of silica glass, which promotes higher Ω_{qtz} , and the use of both rutile and anatase, which promotes a range of initial Ω_{rut} (Cases 2-1, 2-2 and 2-3).

The experiments of TH10 were conducted at higher pressures and they argued that the results can be safely extrapolated to low pressure (Thomas et al., 2015). TH10 interpreted their anatase experiments as having reached quartz-rutile equilibrium even though they grew quartz at much faster rates (tens to hundreds of microns/day) than HA12 (ones to tens of microns/day). The extreme growth rates alone argue against quartz growing from a fluid that is just above saturation, yet as Thomas et al. (2015) point out: “it is unlikely that a nonequilibrium process would have affected [our] results so consistently and systematically to produce the uniform Ti concentrations in quartz from individual experiments, and reproducible P - T dependencies of Ti solubility in quartz.” Case 2-3 provides one way that relatively homogeneous crystals can form with excess Ti, but another possibility is that the fast growth rates alone can give rise to systematic kinetic effects that are not explicitly accounted for in the models.

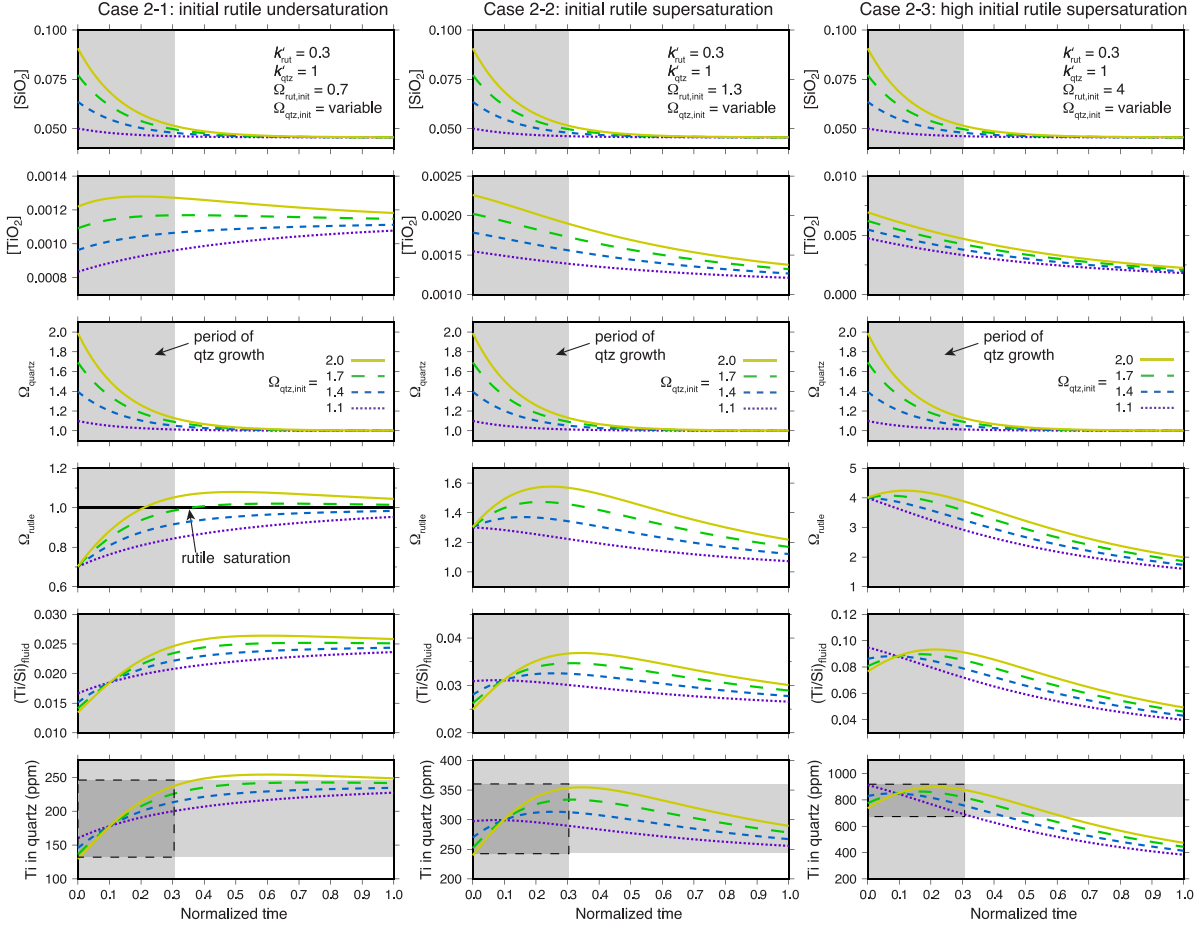


Fig. 11. Model results that incorporate a solubility-dependence of rutile on the SiO_2 content of the fluid. In Case 2-1, the fluid is initially undersaturated in rutile, but Ω_{rutile} increases as the SiO_2 concentration decreases, possibly explaining why the inner capsule overgrowths are coated in rutile but have few rutile inclusions. Case 2-2 shows that widely varying Ti concentrations in quartz can be produced when the fluid is initially supersaturated with respect to both quartz and rutile. Case 2-3 shows that when the fluid is highly supersaturated in rutile, the $\text{TiO}_2/\text{SiO}_2$ ratio remains high throughout the period of quartz precipitation for wide range of Ω_{quartz} values.

5.3. Surface reaction-controlled kinetic effects

The outputs presented above assume a constant partition coefficient such that the crystal has a $\text{TiO}_2/\text{SiO}_2$ ratio that is offset from that of the fluid by a constant amount. This is a crude approximation because the partition coefficient itself is known to depend on the growth rate of the crystal (Watson, 2004; DePaolo, 2011; Watkins et al., 2017). A general expression for the non-equilibrium partition coefficient, K_p , is (DePaolo, 2011):

$$K_p = \left(\frac{a_{\text{TiO}_2}^{\text{qz}} / a_{\text{SiO}_2}^{\text{qz}}}{a_{\text{TiO}_2}^{\text{liquid}} / a_{\text{SiO}_2}^{\text{liquid}}} \right) \approx \frac{K_f}{1 + \frac{R_b}{R_p+R_b} \left(\frac{K_f}{K_{\text{eq}}} - 1 \right)} \quad (11)$$

where K_f is the forward kinetic fractionation factor for $\text{TiO}_2/\text{SiO}_2$ in the precipitation reaction; K_{eq} is the equilibrium $\text{TiO}_2/\text{SiO}_2$ partition coefficient; R_p is the net crystal growth rate (moles/s or moles/ m^2/s , which can be converted to a linear growth rate in m/day using the molar density of quartz); R_b is the gross rate of ion detachment (same units

as R_p). This expression describes a growth rate dependence to trace element uptake between an equilibrium limit at slow growth ($R_p \ll R_b$) and a kinetic limit at fast growth ($R_p \gg R_b$). Such a kinetic limit has been documented for Sr/Ca in calcite without necessarily compromising its utility as a geothermometer (Gabitov and Watson, 2006). The crossover between the two limits occurs at $R_p \sim R_b$, but it is important to note that the functional forms of R_p and R_b can depend on many factors, including the degree of supersaturation, that are not well-known at this point. For Ti in quartz, there is an indication in the data of HA12 that increasing growth rate leads to higher Ti/Si in quartz; i.e., K_f is expected to be greater than K_{eq} .

A mechanistic explanation for the kinetic limit has yet to be developed, but we speculate that it may coincide with the regime where the step velocity (V_{step}) increases linearly with solution saturation (Rashkovich and Kronske, 1997). For laboratory-grown potassium orthophosphate (KDP) crystals, for example, it is observed that at very low oversaturation, crystals are in a “dead zone” where the impurity

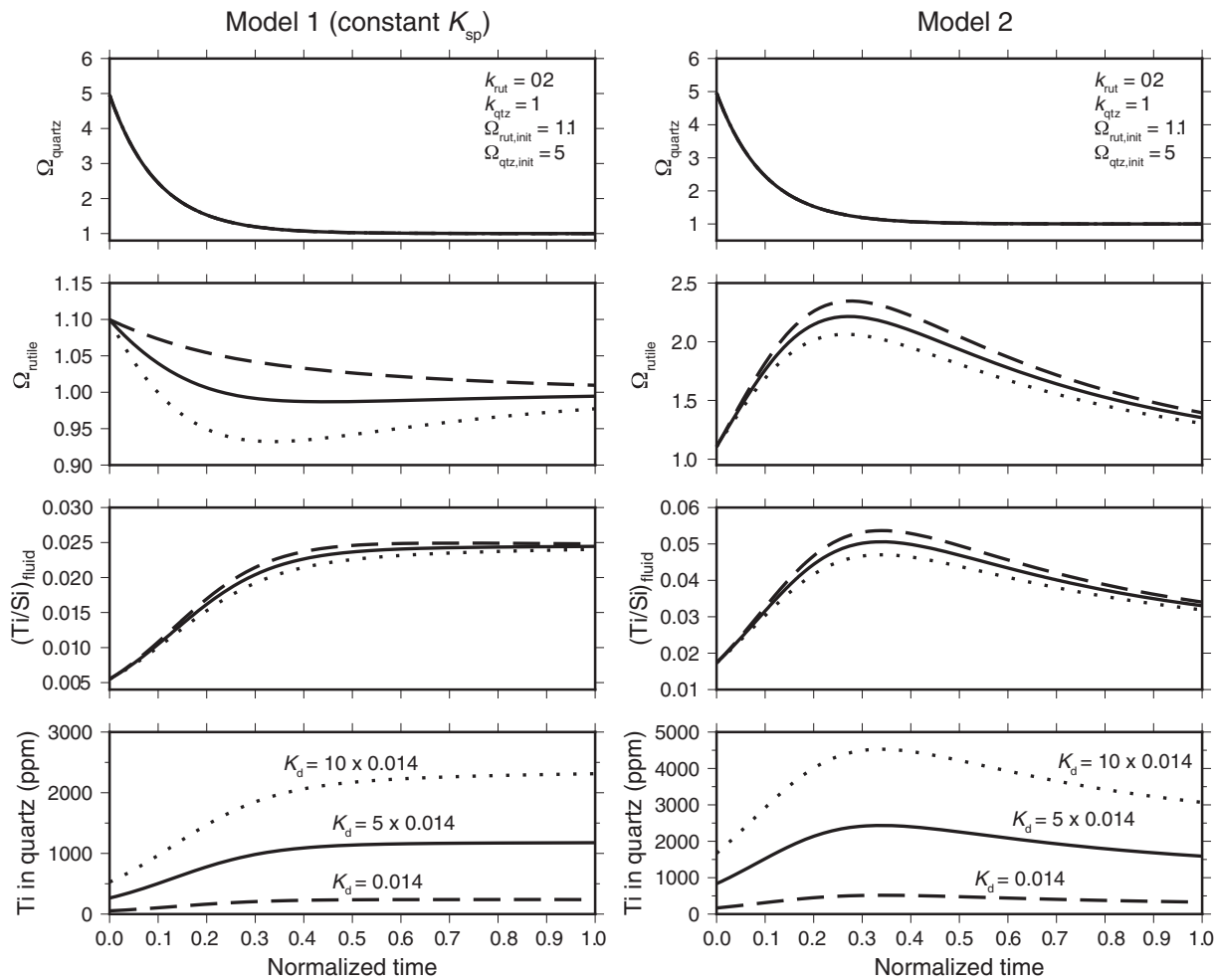


Fig. 12. Model results testing whether TiO_2 incorporation into quartz can lead to rutile undersaturation. According to Model 1, a large degree of quartz supersaturation ($\Omega_{\text{qzt}} = 5$) combined with high K_d (10 times the estimated value) can lead to a small degree of rutile undersaturation from a fluid that is initially slightly above saturation. According to Model 2, once rutile is supersaturated it stays supersaturated.

molecules attached to growth steps inhibit the step advancement. At slightly higher oversaturation, V_{step} increases gradually with Ω , and with further increase in Ω , the $V_{\text{step}}(\Omega)$ curve increases sharply until reaching a critical $\Omega = \Omega^*$, above which $V_{\text{step}}(\Omega)$ is linear. It has been found that crystals grown at lower supersaturation have many defects and fluid inclusions whereas crystals grown rapidly at high supersaturation are have a homogeneous distribution of impurities and are defect-free – traits that could be mistaken for near-equilibrium growth (Zaitseva et al., 1999). If this behavior also applies to hydrothermal quartz, crystallization at low to moderate degrees of supersaturation could explain the abundant cavities and heterogenous Ti concentrations in our run products as well as those from HA12 and may indicate that the high supersaturation linear regime is more accessible at high pressure.

5.4. Solubility of Ti in quartz

Based on all of the considerations discussed herein, we suspect that many of the experimentally grown quartz

crystals are supersaturated with respect to rutile. A certain degree of supersaturation is always required to nucleate and grow a new phase, and the kinetic barrier to spontaneous nucleation of rutile from quartz is likely to be large because the Ti atoms, if uniformly distributed, are separated from each other by tens to hundreds of Si atoms. It thus seems plausible for the quartz lattice to be able to accommodate Ti significantly in excess of the saturation value. In the thermal annealing experiments of TH15, for example, the quartz starting material was supersaturated in TiO_2 by at least a factor of 3–4, and yet, the relict quartz cores retained their high Ti and appear to have not exsolved rutile during the four days they were held at 925 °C and 20 kbar.

A recent study provides additional evidence that the highest experimental Ti concentrations in quartz at a given T and P overestimate the equilibrium solubility value. Nachlas and Hirth (2015) ran dynamic recrystallization experiments involving laboratory-synthesized low-Ti silica gel (110 ppm Ti) and high-Ti silica gel (2280 ppm Ti). The two aggregates were pressed together and then sheared at 10 kbar and 900 °C. Under these conditions, the gel crystal-

lized to quartz and the quartz recrystallized continuously during shear deformation. The equilibrium Ti was expected to be either 310 ppm (TH10) or 101 ppm (HA12), depending on which calibration is used. The high-Ti half exsolved rutile, as expected, and the recrystallized quartz had Ti concentrations broadly overlapping results from HA12 and well below the predictions of TH10. It is difficult to rationalize why the high-Ti side (2280 ppm) of these deformation couples would overshoot the 310 ppm equilibrium value of TH10 if that were the true equilibrium concentration.

5.5. Additional considerations

The TH10 calibration was carried out at high pressures (5–20 kbar) whereas the pressure range over which TitaniQ has been applied to well-constrained samples is considerably lower (1–4 kbar; Supp. table). This raises the question of whether the disagreement between HA12 and TH10 might be caused by an unusual pressure dependence (curved isopleth). A recent calibration by [Zhang et al. \(2020\)](#) using silicate melts instead of solutions suggests that this may in fact be the case and comes close to reconciling the experimental results, though significant discrepancies remain between this calibration and the experiments of HA12, TH10, and [Nachlas and Hirth \(2015\)](#) where they overlap in pressure at 10 kbar. Once the equilibrium solubility and its functional form are more firmly established, the framework we developed herein should prove useful for explaining residual kinetic effects and why different experimental configurations can yield different results.

6. CONCLUSIONS

Our Ti-in-quartz results at 800 °C and 1 kbar span the range of previous calibrations. The two endmember interpretations for the wide range are: (1) the wide range reflects variable degrees of rutile undersaturation ($0 < \Omega_{\text{rut}} < 1$) in a system where extrapolation of the TH10 calibration reflects equilibrium or (2) extrapolation of TH10 overestimates the equilibrium value and the wide range reflects variable degrees of rutile under- and over-saturation ($0 < \Omega_{\text{rut}} < ?$) as quartz grows from variably supersaturated liquids ($1 < \Omega_{\text{qtz}} < 2$).

We developed models to account for the complexities inherent in the experiments, but the only models that appear capable of explaining the textures we observe (incomplete dissolution of rutile starting material, complete dissolution-recrystallization of anatase starting material, rutile inclusions in quartz, and rutile coating the surfaces of quartz) involve slow rutile precipitation rates and a dependence of TiO_2 saturation state on SiO_2 saturation state. The latter effect has been documented in a recent rutile solubility study ([Mysen, 2019](#)). Our conclusion, which is based on application of TitaniQ to natural samples along with our new results and models, is that the HA12 experiments at low pressure are a better analog to natural quartz than extrapolation of the TH10 results at high pressure, indicating that a curved isopleth describes Ti-in-quartz solubility (HA12; [Zhang et al., 2020](#)). More work is needed to

reconcile remaining discrepancies among the various experimental studies and to design and interpret experiments aimed at estimating equilibrium TiO_2 concentrations in quartz.

ACKNOWLEDGEMENTS

We are grateful for reviews from Tom Sisson, Jim Van Orman, Jay Thomas, and three anonymous reviewers. We thank Zack Gainsforth for help with electron diffraction pattern interpretation, as well as Janet Tate and Okan Agirseven for help with Raman spectroscopy. Authors MDA, JMW, and MHR were supported by the National Science Foundation under grant no. EAR1524665. DJD was supported by the US Department of Energy, Office of Science, Office of Basic Energy Sciences under Award No. DE-AC02-05CH11231 to Lawrence Berkeley National Laboratory.

APPENDIX A. SUPPLEMENTARY MATERIAL

Supplementary data to this article can be found online at <https://doi.org/10.1016/j.gca.2020.04.030>.

REFERENCES

- Ackerson M. R., Mysen B. O., Tailby N. D. and Watson E. B. (2018) Low-temperature crystallization of granites and the implications for crustal magmatism. *Nature* **559**, 94–97.
- Antignano A. and Manning C. E. (2008) Rutile solubility in H_2O , $\text{H}_2\text{O}-\text{SiO}_2$, and $\text{H}_2\text{O}-\text{NaAlSi}_3\text{O}_8$ fluids at 0.7–2.0 GPa and 700–1000 °C: Implications for mobility of nominally insoluble elements. *Chem. Geol.* **255**, 283–293.
- Ashley K. T., Webb L. E., Spear F. S. and Thomas J. B. (2013) P-T-D histories from quartz: A case study of the application of the TitaniQ thermobarometer to progressive fabric development in metapelites. *Geochim. Geophys. Geosyst.* **14**, 3821–3843.
- Behr W. M. and Platt J. P. (2011) A naturally constrained stress profile through the middle crust in an extensional terrane. *Earth Planet. Sci. Lett.* **303**, 181–192.
- Bergman H. and Piazolo S. (2012) The recognition of multiple magmatic events and pre-existing deformation zones in metamorphic rocks as illustrated by CL signatures and numerical modelling: examples from the Ballachulish contact aureole, Scotland. *Int. J. Earth Sci.* **101**, 1127–1148.
- Betsi T. B. and Lentz D. R. (2010) The nature of “quartz eyes” hosted by dykes associated with Au-Bi-As-Cu, Mo-Cu, and base-metal-Au-Ag mineral occurrences in the mountain free-gold region (Dawson Range), Yukon Canada. *J. Geosci.* **55**, 347–368.
- Borisova A. Y., Zagrdenov N. R., Toplis M. J., Donovan J. J., Llovet X., Asimow P. D., de Parseval P. and Gouy S. (2018) Secondary fluorescence effects in microbeam analysis and their impacts on geospeedometry and geothermometry. *Chem. Geol.* **490**, 22–29.
- Chamberlain K. J., Morgan D. J. and Wilson C. J. N. (2014) Timescales of mixing and mobilisation in the Bishop Tuff magma body: perspectives from diffusion chronometry. *Contrib. to Mineral. Petrol.* **168**, 1034.
- De Yoreo J. J., Zepeda-Ruiz L. A., Friddle R. W., Qiu S. R., Wasylewski L. E., Chernov A. A., Gilmer G. H. and Dove P. M. (2009) Rethinking classical crystal growth models through molecular scale insights: consequences of kink-limited kinetics. *Crystal Growth Design* **9**(12), 5135–5144.

- DePaolo D. J. (2011) Surface kinetic model for isotopic and trace element fractionation during precipitation of calcite from aqueous solutions. *Geochim. Cosmochim. Acta* **75**, 1039–1056.
- Donovan J. J., Lowers H. A. and Rusk B. G. (2011) Improved electron probe microanalysis of trace elements in quartz. *Am. Mineral.* **96**(2–3), 274–282.
- Donovan J. J., Singer J. W. and Armstrong J. T. (2016) A new EPMA method for fast trace element analysis in simple matrices. *Am. Mineral.* **101**, 1839–1853.
- Gabitov R. I. and Watson E. B. (2006) Partitioning of strontium between calcite and fluid. *Geochem., Geophys., Geosyst.* **7**(11).
- Ghiorso M. S. and Evans B. W. (2008) Thermodynamics of rhombohedral oxide solid solutions and a revision of the Fe-Ti two-oxide geothermometer and oxygen-barometer. *Am. J. Sci.* **308**, 957–1039.
- Girard G. and Stix J. (2012) Future volcanism at Yellowstone caldera: Insights from geochemistry of young volcanic units and monitoring of volcanic unrest. *GSA Today* **22**, 4–10.
- Gouma P. I. and Mills M. J. (2001) Anatase-to-Rutile Transformation in Titania Powders. *J. Am. Ceram. Soc.* **84**, 619–622.
- Hanaor D. A. H. and Sorrell C. C. (2011) Review of the anatase to rutile phase transformation. *J. Mater. Sci.* **46**, 855–874.
- Huang R. and Audébat A. (2012) The titanium-in-quartz (TitaniQ) thermobarometer: A critical examination and re-calibration. *Geochim. Cosmochim. Acta* **84**, 75–89.
- Johnson J., Oelkers E. and Helgeson H. (1992) SUPCRT92: A software package for calculating the standard molal thermodynamic properties of minerals, gases, aqueous species, and reactions from 1 to 5000 bar and 0 to 1000°C. *Comput. Geosci.* **18**, 899–947.
- Kalyani V., Vasile B. S., Ianculescu A., Testino A., Carino A., Buscaglia M. T., Buscaglia V. and Nanni P. (2015) Hydrothermal Synthesis of SrTiO₃: Role of Interfaces. *Cryst. Growth Des.* **15**, 5712–5725.
- Kularatne K. and Audébat A. (2014) Rutile solubility in hydrous rhyolite melts at 750–900°C and 2 kbar, with application to titanium-in-quartz (TitaniQ) thermobarometry. *Geochim. Cosmochim. Acta* **125**, 196–209 <https://www.sciencedirect.com/science/article/pii/S0016703713005760>.
- Lowers, H.A., 2007. Application of the titaniq geothermometer. GSA Denver Annu. Meet., 80225. Available at: https://gsa.confex.com/gsa/2007AM/finalprogram/abstract_129097.htm.
- Mercer C. N. and Reed M. H. (2013) Porphyry Cu-Mo stockwork formation by dynamic, transient hydrothermal pulses: Mineralogic insights from the deposit at Butte, Montana. *Econ. Geol.* **108**, 1347–1377.
- Müller A., Herrington R., Armstrong R., Seltmann R., Kirwin D. J., Stenina N. G. and Kronz A. (2010) Trace elements and cathodoluminescence of quartz in stockwork veins of Mongolian porphyry-style deposits. *Miner. Depos.* **45**, 707–727.
- Mysen B. (2019) Aqueous fluids as transport medium at high pressure and temperature: Ti⁴⁺ solubility, solution mechanisms, and fluid composition. *Chem. Geol.* **505**, 57–65.
- Nachlas W. O. and Hirth G. (2015) Experimental constraints on the role of dynamic recrystallization on resetting the Ti-in-quartz thermobarometer. *J. Geophys. Res. Solid Earth* **120**, 8120–8137.
- Nielsen L. C., De Yoreo J. J. and DePaolo D. J. (2013) General model for calcite growth kinetics in the presence of impurity ions. *Geochimica et Cosmochimica Acta* **115**, 100–114.
- Okada K., Yamamoto N., Kameshima Y., Yasumori A. and MacKenzie K. J. D. (2001) Effect of Silica Additive on the Anatase-to-Rutile Phase Transition. *J. Am. Ceram. Soc.* **84**, 1591–1596.
- Ostapenko G. T., Gamarnik M. Y., Gorogotskaya L. I., Kuznetsov G. V., Tarashchan A. N. and Timoshkova L. P. (1987) Isomorphism of titanium substitution for silicon in quartz: experimental data. *Mineral Zh.* **9**, 30–40.
- Ostapenko G. T., Tarashchan A. N. and Mitsyuk B. M. (2007) Rutile-quartz geothermobarometer. *Geochem. Int.* **45**(5), 506–508.
- Rashkovich L. N. and Kronske N. V. (1997) Influence of Fe³⁺ and Al³⁺ ions on the kinetics of steps on the {1 0 0} faces of KDP. *J. Crystal Growth* **182**(3–4), 434–441.
- Sabyrov K., Burrows N. D. and Penn R. L. (2013) Size-dependent anatase to rutile phase transformation and particle growth. *Chem. Mater.* **25**, 1408–1415.
- Shane P., Smith V. C. and Nairn I. (2008) Millennial timescale resolution of rhyolite magma recharge at Tarawera volcano: insights from quartz chemistry and melt inclusions. *Contrib. to Mineral. Petrol.* **156**, 397–411.
- Shannon R. D. and Pask J. A. (1965) Kinetics of the anatase-rutile transformation. *J. Am. Ceram. Soc.* **48**, 391–398.
- Tanner D., Henley R. W., Mavrogenes J. A. and Holden P. (2013) Combining in situ isotopic, trace element and textural analyses of quartz from four magmatic-hydrothermal ore deposits. *Contrib. to Mineral. Petrol.* **166**, 1119–1142.
- Tesoriero A. J. and Pankow J. F. (1996) Solid solution partitioning of Sr²⁺, Ba²⁺, and Cd²⁺ to calcite. *Geochimica et Cosmochimica Acta* **60**(6), 1053–1063.
- Thomas J. B., Bruce Watson E., Spear F. S., Shemella P. T., Nayak S. K. and Lanzirotti A. (2010) TitaniQ under pressure: the effect of pressure and temperature on the solubility of Ti in quartz. *Contrib. to Mineral. Petrol.* **160**, 743–759.
- Thomas J. B., Watson E. B., Spear F. S. and Wark D. A. (2015) TitaniQ recrystallized: experimental confirmation of the original Ti-in-quartz calibrations. *Contrib. to Mineral. Petrol.* **169**, 27.
- Vasyukova O. V., Goemann K., Kamenetsky V. S., MacRae C. M. and Wilson N. C. (2013) Cathodoluminescence properties of quartz eyes from porphyry-type deposits: Implications for the origin of quartz. *Am. Mineralog.* **98**(1), 98–109.
- Walther J. V. and Helgeson H. C. (1977) Calculation of the thermodynamic properties of aqueous silica and the solubility of quartz and its polymorphs at high pressures and temperatures. *Am. J. Sci.* **277**, 1315–1351.
- Wark D. A., Hildreth W., Spear F. S., Cherniak D. J. and Watson E. B. (2007) Pre-eruption recharge of the Bishop magma system. *Geology* **35**, 235–238.
- Wark D. A. and Watson E. B. (2006) TitaniQ: a titanium-in-quartz geothermometer. *Contrib. to Mineral. Petrol.* **152**, 743–754.
- Watkins J. M., DePaolo D. J. and Watson E. B. (2017) Kinetic Fractionation of Non-Traditional Stable Isotopes by Diffusion and Crystal Growth Reactions. *Rev. Mineral. Geochem.* **82**, 85–125.
- Watson B. E. (2004) A conceptual model for near-surface kinetic controls on the trace-element and stable isotope composition of abiogenic calcite crystals. *Geochim. Cosmochim. Acta* **68**, 1473–1488.
- Zaitseva N., Carman L., Smolsky I., Torres R. and Yan M. (1999) The effect of impurities and supersaturation on the rapid growth of KDP crystals. *J. Crystal Growth* **204**(4), 512–524.
- Zhang H. and Banfield J. F. (1999) New kinetic model for the nanocrystalline anatase-to-rutile transformation revealing rate dependence on number of particles. *Am. Mineral.* **84**, 528–535.
- Zhang C., Li X., Almeev R. R., Horn I., Behrens H. and Holtz F. (2020) Ti-in-quartz thermobarometry and TiO₂ solubility in rhyolitic melts: New experiments and parametrization. *Earth Planetary Sci. Lett.* **538** 116213.